Factor Learning Portfolio Optimization Informed by Continuous-Time Finance Models

Sinong Geng
Princeton University

Houssam Nassif
Meta

Zhaobin Kuang
Stanford University

Anders Max Reppen
Boston University

Ronnie Sircar
Princeton University

Reviewed on OpenReview: *https://openreview.net/forum?id=KLOJUGusVE*

Abstract

This work considers financial portfolio optimization in the presence of unknown and uncontrolled system variables referred to as stochastic factors. Existing work falls into two contrasting distinct categories: (i) Reinforcement learning employs end-to-end policy learning with flexible factor representation, but does not precisely model the dynamics of asset prices or factors; (ii) Continuous-time finance methods take advantage of explicitly modeled dynamics but pre-specify, rather than learn, factor representation. We propose FaLPO (**Fa**ctor **L**earning **P**ortfolio **O**ptimization), a framework that interpolates between these two approaches. Specifically, FaLPO hinges on deep policy gradient to learn a performant investment policy that takes advantage of flexible representation for stochastic factors. FaLPO also incorporates continuous-time finance models when modeling the dynamics. It uses the optimal policy functional form derived from such models and optimizes an objective that combines policy learning and model calibration. We prove the convergence of FaLPO and provide performance guarantees via a finite-sample bound. On both synthetic and real-world portfolio optimization tasks, we observe that FaLPO outperforms five leading methods. Finally, we show that FaLPO can be extended to other decision-making problems with stochastic factors.

1 Introduction

Portfolio optimization studies how to allocate investments across multiple risky financial assets (such as stocks) and safe assets (such as US government bonds). The investment target is often formulated as maximizing the expected *utility* of the investment portfolio's value at a fixed time horizon, which conceptually maximizes profit while constraining risk (von Neumann & Morgenstern, 1947). With continuous-time stochastic models of stock prices, great advances in the expected utility maximization framework were made in Merton (1969) using stochastic optimal control (dynamic programming) methods. More realistic models incorporate *factors* like economic indices and proprietary trading signals (Merton et al., 1973; Fama & French, 2015; 1992), which (i) affect the dynamics of stock prices; (ii) stochastically evolve over time; (iii) are not affected by individual investment decisions. With greater data availability, it is natural to design and apply data-driven

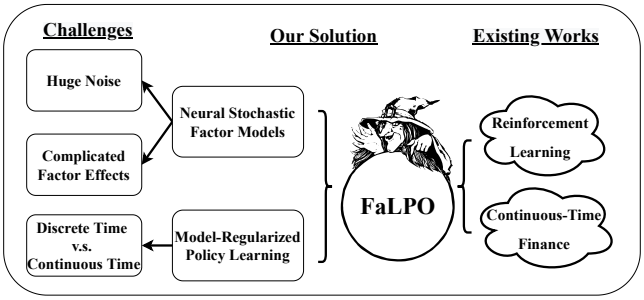

Figure 1: Demonstration of FaLPO

machine learning methods (Bengio, 1997; Dixon et al., 2020; De Prado, 2018) to handle factors for portfolio optimization. This work proposes a novel method—(**Fa**ctor **L**earning **P**ortfolio **O**ptimization)—which combines tools from both machine learning and continuous-time finance.

Portfolio optimization with stochastic factors is challenging for three reasons. First, financial data is notoriously noisy and idiosyncratic (Goyal & Santa-Clara, 2003), causing complex purely data-driven methods to be unstable and prone to overfitting. Second, the relationship between the factors and their impact on stock prices can be extremely complicated and difficult to model *ex ante*. Third, many successful finance models are in continuous time and require interacting with the environment infinitely frequently. As a result, such models cannot be easily combined with machine learning methods, many of which are in discrete time.

Current approaches to portfolio optimization broadly fall into two categories: reinforcement learning (RL) and continuous-time finance methods. Many RL solutions to portfolio optimization are built on deep deterministic policy gradient methods (Silver et al. 2014; Hambly et al. 2023, Section 4.3). Such methods parameterize the policy function as a neural network that takes factors as input and learns the neural network by optimizing the corresponding portfolio performance. However, these approaches (as well as other model-free methods like Haarnoja et al. 2018; Geng et al. 2024) have high sample complexity and tend to overfit due to the high noise in the data. Other RL methods explicitly learn representation (Watter et al., 2015; Lee et al., 2020; Laskin et al., 2021) and leverage discrete-time models (Deisenroth & Rasmussen, 2011; Gu et al., 2016; Mhammedi et al., 2020; Janner et al., 2019; Nagabandi et al., 2018). Nonetheless, these methods are not informed by continuous-time finance models and, as our experiments suggest in Section 5, cannot benefit from structures inherent in the financial market. As a result, RL provides flexible representation for stochastic factors but suffers from the high noise in the data.

Stochastic factor models can be used to mathematically derive optimal (or approximately optimal) investment policies (Kim & Omberg, 1996; Chacko & Viceira, 2005; Fouque et al., 2017; Avanesyan, 2021). To this end, one needs domain knowledge to pick and model the factors. Then, *model calibration* (a.k.a. model fitting, parameter estimation) is conducted by maximizing a calibration objective. With the calibrated model, the optimal investment policy can be derived analytically or numerically (Merton, 1992; Fleming & Soner, 2006). This procedure of calibration and optimization effectively constrains the 'learning' in the optimization step, and thus helps reduce overfitting to noisy data. However, this approach cannot capture the complicated factor effects in the data, because the factors may be complex and unlikely to be identified manually. Therefore, these methods may end up with oversimplified models and suffer from model bias with suboptimal performance.

To tackle these limitations, we propose factor learning portfolio optimization (FaLPO), a new method that interpolates between the two aforementioned solutions (Figure 1). FaLPO includes (i) a neural stochastic factor model to handle huge noise and complicated factor effects, and (ii) a model-regularized policy learning method to combine continuous-time models with discrete-time policy learning methods. First, to reduce the sample complexity and avoid overfitting, FaLPO assumes factors and asset prices follow a parametric continuous-time finance model. To capture the complicated factor effects, FaLPO models the factors by a representation function ϕ parameterized by a neural network with minimal parametric constraints. Second, for policy learning, FaLPO incorporates two types of regularization derived from continuous-time stochastic

factor models: a policy functional form and model calibration. Specifically, we derive policy functional forms from the neural stochastic factor model using stochastic optimal control tools, and apply it to parameterize the candidate policy in FaLPO. The use of this form in the learning algorithm effectively acts as a regularizer. Then, model calibration and policy learning are conducted jointly, such that the learned policy is informed by continuous-time models.

Theoretically, we prove that the added continuous-time regularization leads to the optimal portfolio performance as the trading frequency increases. Empirically, we demonstrate the improved performance of the proposed method by both synthetic and real-world experiments. We review the related literature in Appendix A. We also discuss how FaLPO is extendable beyond portfolio optimization, and can be applied to other decision-making problems with stochastic factors in Appendix H.

2 Background

In this section, we first formulate the portfolio optimization problem. We then review two major solutions to this problem: deep deterministic policy gradient in reinforcement learning (RL), and stochastic factor models in continuous-time finance.

2.1 Portfolio Optimization

Problem Formulation Portfolio optimization seeks to derive a policy of asset allocation that yields high return while maintaining low risk for the investment. Formally, consider d_S risky assets with prices $S_t := [S_t^1, S_t^2, \cdots S_t^{d_S}]^\top$ and a risk-free money market account with, for simplicity, zero interest rate of return (like cash). We observe d_Y stochastic factors (e.g. economic indices, market benchmarks) denoted as Y_t. Such stochastic factors (i) affect the dynamics of asset prices; (ii) evolve over time stochastically; (iii) are not affected by investment decisions. Given an initial investment capital (or wealth) z_0 and the initial values for Y_t and S_t as y_0 and s_0, we use a $d_S \times 1$ vector π_t to denote the fractions of wealth invested in the d_S assets at time point t. Note that negative values are allowed in π_t indicating short positions. At the terminal time $T > 0$, the target is to maximize the expectation of a given utility function $\mathbb{E}[U(Z_T^\pi)]$,

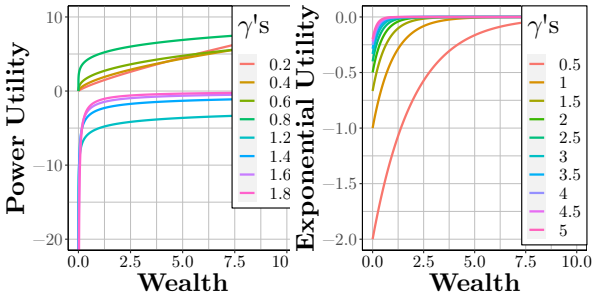

Figure 2: Power and exponential utilities.

Intuitively, a utility function reflects the risk preference of an investor. It is an increasing function of wealth that is also concave: it changes significantly when the wealth is low but less so when the wealth is high (Figure 2). This work focuses on the power utility $U(z;\gamma) := \frac{1}{1-\gamma} z^{1-\gamma}$ with $\mathcal{Z} = \mathbb{R}^+$, $\gamma > 0$, and $\gamma \neq 1$; and the exponential utility $U(z;\gamma) := -\frac{\exp(-\gamma z)}{\gamma}$ with $\mathcal{Z} = \mathbb{R}$ and $\gamma > 0$. Here, γ is the investor's risk aversion coefficient and is hand-picked (instead of tuned) by the user. A larger γ corresponds to more risk aversion, while a smaller γ corresponds to more risk tolerance. Note that potentially, one can learn a suitable γ from data, which is related to inverse reinforcement learning (Geng et al., 2020; 2023). Our method is also applicable to other utility functions and other objective functions for portfolio optimization (see Appendix B).

Discrete- and Continuous-Time Policies Discrete- and continuous-time policies are two major types of investment policies, differing on how frequently the portfolio is rebalanced. A discrete-time policy rebalances the portfolio finitely frequently, leading to a discrete-time dynamics for the wealth. Such policies are often considered in RL methods (Section 2.2). Continuous-time policies rebalance the investment infinitely frequently, leading to a continuous-time dynamics for the wealth. These policies are often found explicitly in continuous-time finance models (Section 2.3)[1].

[1]It is impossible to rebalance a portfolio infinitely frequently in practice, continuous-time policies are mostly analytical tools.

2.2 Deep Deterministic Policy Gradient

We review deep deterministic policy gradient (DDPG, Silver et al. 2014)—a quintessential example of RL methods. DDPG does not explicitly model the dynamics, but instead directly learns a discrete-time policy for portfolio optimization. DDPG parameterizes the policy function as a deep neural network and conducts gradient-based policy learning. Denote by $\pi(t, S_t, Z_t, Y_t; \theta_D)$ the deep policy function with parameter θ_D. Without explicitly modeling the dynamics of S_t or X_t, DDPG directly maximizes the following performance objective to learn a policy:

$$\max_{\theta_D} V(\theta_D) \text{ with } V(\theta_D) := \mathbb{E}[U(Z_T^{\pi(\cdot;\theta_D)})], \tag{1}$$

where the expectation is over the terminal wealth $Z_T^{\pi(\cdot;\theta_D)}$ following the policy $\pi(\cdot;\theta_D)$. A key step is to compute the gradient of $V(\theta_D)$ to update θ_D. Following the procedure in Appendix C, this can be achieved by sampling the trajectories of S_t and Y_t to approximate the expectation and thus the gradient of $V(\theta_D)$.

Typically, DDPG learns a discrete-time policy that rebalances the portfolio finitely frequently. To see how the policy rebalances the portfolio, we study its corresponding wealth process $Z_t^{\pi(\cdot;\theta_D)}$ that characterizes the changes in wealth over time. Let $\Delta t > 0$ be the time interval (e.g. daily, weekly) to rebalance the portfolio and, for integer $M > 0$, let $T := M\Delta t$ be the fixed investment horizon (e.g. one or two months). At time $m\Delta t$ with $m \in \{0, 1, 2, \cdots, M-1\}$, define $\pi^i_{m\Delta t} := \pi^i(m\Delta t, S_{m\Delta t}, Z_{m\Delta t}, Y_{m\Delta t}; \theta_D)$ as the fraction of current wealth invested in the ith risky asset. Then, the wealth change at time $m\Delta t$ is: $Z^{\pi(\cdot;\theta_D)}_{(m+1)\Delta t} - Z^{\pi(\cdot;\theta_D)}_{m\Delta t} = Z^{\pi(\cdot;\theta_D)}_{m\Delta t}\left[\sum_{i=1}^{d_S} \pi^i_{m\Delta t}\frac{S^i_{(m+1)\Delta t} - S^i_{m\Delta t}}{S^i_{m\Delta t}}\right]$, where $Z^{\pi(\cdot;\theta_D)}_{m\Delta t}\pi^i_{m\Delta t}\frac{S^i_{(m+1)\Delta t} - S^i_{m\Delta t}}{S^i_{m\Delta t}}$ is the wealth change due to the investment in the ith risky asset. Note that the number of shares invested in an asset ($Z^{\pi(\cdot;\theta_D)}_{m\Delta t}\frac{\pi^i_{m\Delta t}}{S^i_{m\Delta t}}$) does not change during $(m\Delta t, (m+1)\Delta t)$: the portfolio rebalances every Δt time.

RL methods like DDPG provide flexible representation for factors: the hidden layers of the neural network are considered as the representation learned for Y_t, providing strong representation power. Nonetheless, RL methods do not provide an explicit parametric model for the learned representation and asset prices. Consequently, such methods require lots of data and tend to overfit (Aboussalah et al., 2022).

2.3 Stochastic Factor Models

We review stochastic factor models in continuous-time finance. These models can explicitly formulate the dynamics and can also be used to mathematically derive the functional form of the optimal continuous-time investment policy. Stochastic factor models are described by stochastic differential equations (SDEs) (see Oksendal 2013 and Appendix D) to formulate the dynamics of asset prices S_t. Specifically, let $W_t := [W_t^1, W_t^2, \cdots W_t^{d_W}]^\top$ be a $d_W \times 1$ Brownian motion that characterizes random fluctuations. Let $i \in \{1, 2, \cdots, d_S\}$. Then, S_t and Y_t are assumed to follow

$$\begin{aligned} \frac{dS_t^i}{S_t^i} &= f_S^i(Y_t; \theta_S^*)dt + \sum_{j=1}^{d_W} g_S^{ij}(Y_t; \theta_S^*)dW_t^j, \\ dY_t &= f_Y(Y_t; \theta_S^*)dt + g_Y(Y_t; \theta_S^*)^\top dW_t. \end{aligned} \tag{2}$$

In Equation (2), $f_S : \mathbb{R}^{d_Y} \to \mathbb{R}^{d_S}$, $f_Y : \mathbb{R}^{d_Y} \to \mathbb{R}^{d_Y}$, $g_S : \mathbb{R}^{d_Y} \to \mathbb{R}^{d_S \times d_W}$, and $g_Y : \mathbb{R}^{d_Y} \to \mathbb{R}^{d_Y \times d_W}$ are parametric functions pre-specified by domain knowledge. Further, f_S and f_Y are often referred to as the drift, and g_S and g_Y as the volatility of S_t and Y_t respectively. Intuitively, SDEs formulate the change of a variable in an infinitesimal time step as the sum of a deterministic part (dt) and a stochastic part (dW_t), and we use θ_S^* to parameterize the SDE. The factor Y_t appears in both the drift and volatility of the asset prices, thus affecting the price transition. With the parametric functional forms in Equation (2), we can use tools in stochastic optimal control to derive the functional form of the optimal continuous-time investment policy.

Continuous-time policies change the investment in each asset at every time point. For a continuous-time investment policy $\tilde{\pi}_t$, the dynamics of wealth $\tilde{Z}_t^{\tilde{\pi}}$ is defined as $\frac{d\tilde{Z}_t^{\tilde{\pi}}}{\tilde{Z}_t^{\tilde{\pi}}} := \sum_{i=1}^{d_S} \frac{\tilde{\pi}_t^i dS_t^i}{S_t^i}$, with $\tilde{Z}_0 = z_0$, $S_0 =$

s_0 and $Y_0 = y_0$. Crucially, this is different from the discrete-time wealth process Z_t^π in Section 2.2, as the number of shares $\frac{\tilde{Z}_t^{\tilde{\pi}} \tilde{\pi}_t^i}{S_t^i}$ in asset i now changes continuously over time, as opposed to being rebalanced at finite intervals. This discrepancy creates obstacles to directly apply the results derived from stochastic factor models to discrete-time policy learning.

Stochastic factor models can reduce sample complexity for portfolio optimization, since the assumed functional forms in Equation (2) significantly constrain the solution space. However, a crucial step to apply stochastic factor models is to pick or even construct Y_t that perfectly follows a pre-specified model. This step often relies on domain knowledge and thus may end up with oversimplified models suffering from model bias and eventually leading to suboptimal performance.

3 Factor Learning Portfolio Optimization

We now propose factor learning portfolio optimization (FaLPO), a new decision-making framework that interpolates between DDPG and stochastic factor models. FaLPO has two components: (i) a neural stochastic factor model to handle huge noise and complicated factor effects and (ii) model-regularized policy learning to combine continuous-time models with discrete-time policy learning methods.

3.1 Neural Stochastic Factor Models

We describe neural stochastic factor models (NSFM) and discuss their benefits. Specifically, a neural stochastic factor model is defined as

$$\begin{aligned} \frac{dS_t^i}{S_t^i} &= f_S^i(X_t; \theta_S^*)dt + \sum_{j=1}^{d_W} g_S^{ij}(X_t; \theta_S^*)dW_t^j, \\ dX_t &= f_X(X_t; \theta_S^*)dt + g_X(X_t; \theta_S^*)^\top dW_t, \\ X_t &= \phi(Y_t; \theta_\phi^*). \end{aligned}$$

On the one hand, a neural stochastic factor model assumes the existence of a representation function ϕ for factors such that $X_t = \phi(Y_t; \theta_\phi^*)$ along with asset prices S_t follows a stochastic factor model (e.g. Equations (2) and (6)), which reduces the sample complexity and avoids overfitting. On the other hand, ϕ is formulated as a neural network with parameter θ_ϕ^*. As a result, FaLPO avoids hand-picking factors following SDEs as is the case in stochastic factor models (Section 2.3). The neural network representation has only a few parametric constraints and thus is able to capture complicated factor effects in the data. Note that the notation of X_t is only provided for the ease of exposition: it does *not* represent any external data other than the factors Y_t. A demonstration of NSFM is provided in Figure 3.

3.2 Model-Regularized Policy Learning

Under the proposed neural stochastic factor model, we aim to learn the discrete-time optimal policy function π_t^* and the representation function $\phi(\cdot; \theta_\phi^*)$. However, while the policy learning is for discrete-time policies, our proposed model is in continuous time. To bridge this gap, we incorporate two types of continuous-time model regularization into discrete-time policy learning: (i) the policy functional form of Equation (3) and (ii) the model calibration objective of Equation (4).

Policy Functional Form From our model, we apply the functional form of a continuous-time optimal policy into our discrete-time policy learning. Using tools in stochastic optimal control, we can derive the functional form of an optimal continuous-time policy: $\tilde{\pi}_t^* = \Pi(t, S_t, Z_t, X_t; \theta_{\tilde{\pi}}^*)$, where the functional form of Π can be obtained in many existing stochastic factor models (Kim & Omberg, 1996; Chacko & Viceira, 2005; Avanesyan, 2021; Zariphopoulou, 2001; Wachter, 2002; Kraft, 2005), and $\theta_{\tilde{\pi}}^*$ is an optimal parameter for Π. FaLPO uses the functional form of Π in policy learning and parameterize the candidate policy as

$$\pi(t, S_t, Z_t, Y_t; \theta_\phi, \theta_\pi) := \Pi(t, S_t, Z_t, \phi(Y_t; \theta_\phi); \theta_\pi), \tag{3}$$

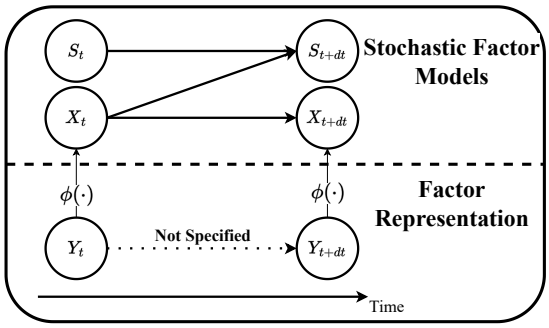

Figure 3: Demonstration for neural stochastic factor models.

Algorithm 1 FaLPO Algorithm

1: **Input:** number of iterations N.
2: Initialize θ_ϕ and θ_π .
3: **for** $n \in [N]$ **do**
4: Parameterize the policy function according to Equation (3).
5: Estimate the policy gradient for H in Equation (5) (Appendix C).
6: Update θ_ϕ, θ_π, and θ_S.
7: **end for**
8: **Return** $\pi(\cdot; \boldsymbol{\theta}_\phi, \boldsymbol{\theta}_\pi)$

where ϕ is the representation function for the factors in Section 3.1. As a result, Π constrains the policy space and acts as regularization. Importantly, although Π is derived for continuous-time policies, it can still provide guidance for discrete-time policy learning when Δt is small. We rigorously prove the soundness of using Equation (3) in Section 4.

Model Calibration FaLPO also hinges on model calibration to regularize policy learning. Given the specific functional forms in (2), FaLPO conducts model calibration to estimate the parameters of the SDE. The calibration procedure can be summarized as maximizing a model calibration objective:

$$\max_{\theta_S} L(\theta_\phi, \theta_S). \tag{4}$$

In practice, with discrete data, one may use likelihood (Phillips, 1972; Beskos & Roberts, 2005) or other likelihood-based objective functions (Bishwal, 2007; Aït-Sahalia & Kimmel, 2010) for L (see Appendix E for concrete examples).

To harness the information provided by model calibration in policy learning, FaLPO combines the model calibration objective L in Equation (4) with the performance objective V in Equation (1), and facilitates a joint optimization over the two. Note that naively combining $L(\theta_\phi, \theta_S)$ and $V(\theta_D)$ is not effective since the two in general do not share common parameters: the parameter of the policy network θ_D has no overlap with the SDE parameter θ_S or factor representation parameter θ_ϕ. However, by constraining the policy space to Equation (3) in FaLPO, we can show that θ_ϕ is also part of the policy parameterization. Thus, V can be derived as $V(\theta_\phi, \theta_\pi) := \mathbb{E}[U(Z_T^{\pi(\cdot;\theta_\phi,\theta_\pi)})]$. In other words, θ_ϕ is shared in both V and L, and hence FaLPO can carry out a joint optimization over the two:

$$\begin{aligned} &\max_{(\theta_\phi,\theta_\pi\theta_S)\in\mathcal{A}} H(\theta_\phi, \theta_\pi, \theta_S), \text{ with} \\ &H(\theta_\phi, \theta_\pi, \theta_S) := (1-\lambda)V(\theta_\phi, \theta_\pi) + \lambda L(\theta_\phi, \theta_S), \end{aligned} \tag{5}$$

where the candidate policy follows the functional form of the optimal continuous-time policy Equation (3) (see Algorithm 1), and $\mathcal{A}$ denotes the considered parameter set. The model calibration objective also acts as a model regularization, where $\lambda \in (0, 1)$ is a hyperparameter determining its effect. In practice, we can

optimize Equation (5) by gradient-based methods, facilitating a easy and end-to-end learning procedure (see Appendix C for gradient estimation details).

3.3 FaLPO example

In portfolio optimization, one can use different types of stochastic factor models. FaLPO can be applied to many such types (see Appendix F). In this section, we use the Kim–Omberg model (Kim & Omberg, 1996) as an example to illustrate FaLPO's modeling and policy learning. Kim–Omberg is a standard model for portfolio optimization with stocahstic factors, which has been extensively studied empirically (Welch & Goyal, 2008; Muhle-Karbe et al., 2017). For modeling, FaLPO with Kim–Omberg model formulates the dynamics of asset prices and factors as

$$\begin{aligned} \frac{dS_t^i}{S_t^i} &= X_t^i\, dt + \sum_{j=1}^{d_W} \sigma^{ij}\, dW_t^j, \\ dX_t &= \mu(\omega - X_t)\, dt + v\, dW_t, \text{ and } X_t = \phi(Y_t; \theta_\phi^*), \end{aligned} \tag{6}$$

where SDE parameters ω, σ, v, and μ are constant matrices or vectors.

For policy learning, we detail the policy functional form and model calibration. Under the Kim-Omberg model, we can derive the optimal policy functional form Π in Equation (3). Specifically, for power utility $\Pi(t, S_t, Z_t, \phi(Y_t; \theta_\phi); \theta_\pi) = k_1(t; \theta_\pi)\phi(Y_t; \theta_\phi) + k_2(t; \theta_\pi)$, for exponential utility $\Pi(t, S_t, Z_t, \phi(Y_t; \theta_\phi); \theta_\pi) = k_1(t; \theta_\pi)\phi(Y_t; \theta_\phi)/Z_t + k_2(t; \theta_\pi)/Z_t$, where $k_1(\cdot; \theta_\pi) : [0, T] \to \mathbb{R}^{d_S \times d_X}$ and $k_2(\cdot; \theta_\pi) : [0, T] \to \mathbb{R}^{d_S \times d_X}$ are two time dependent functions (Appendix F.2). We can derive the functional forms of k_1 and k_2 since the two are solutions to systems of ODEs related to algebraic Riccati equations (Appendix G). We can also directly use function approximators like neural networks or kernel methods for the two. For model calibration, we use a negative mean square loss with the derivation deferred to Appendix E: $L(\theta_\phi, \theta_S) := -\mathbb{E}\left[\sum_{i=1}^{d_S} \left[\log(S_{t+\Delta t}^i) - \log(S_t^i) - \phi^i(Y_t; \theta_\phi)\Delta t - \theta_S^i\right]^2\right]$, where in this case θ_S is a $d_S \times 1$ vector. Therefore, to implement FaLPO, we can parameterize the candidate policy function using Π and optimize Equation (5).

Note that the methodology of FaLPO is also generally applicable to other decision-making problems besides portfolio optimization. In Appendix H, we use linear quadratic control with stochastic factors as an example to demonstrate the generality of FaLPO.

4 Theory

We theoretically analyze both the asymptotic and non-asymptotic characteristics of FaLPO.

4.1 Asymptotic Analysis

FaLPO applies the policy functional form and model calibration derived from continuous-time models to discrete-time policy learning. We show that FaLPO can achieve the optimal performance asymptotically (i.e. with infinite data and perfect optimization). In the following, we describe the assumptions and results and provide the formal theorem in the end.

We provide an intuitive description on the assumptions, with the formal statements provided in Appendix I.1. First, we assume that the portfolio optimization problem satisfies some standard regularity conditions (Higham et al., 2002): the drift and volatility are locally Lipschitz continuous; meanwhile, the asset prices, the stochastic factors, and the wealth process under the optimal policy have bounded moments. Second, we assume that the utility function $U(z)$ has linear growth on $z \in \mathcal{Z}$. Note that some widely used cases like power utility with $\gamma < 1$ and exponential utility with lower-bounded wealth satisfy this assumption. Third, we consider only admissible policies with parameters in $\mathcal{A}$ and we assume that $\mathcal{A}$ covers the optimal continuous-time policy parameter. A policy is admissible if it is predictable and if the wealth process $Z_t^\pi \in \mathcal{Z}$ for any $t \in [0, T]$ almost surely. It is a common practice to only consider such admissible policies in portfolio optimization.

The last two assumptions are artifacts of the current theoretical analysis; in practice FaLPO can achieve reasonable performance without enforcing them (see Section 5).

With the foregoing assumptions, we show that the performance of FaLPO can asymptotically converge to that of the best policy in discrete time. Define $V^*_{\Delta t} := V(\pi^*)$ where π^* is an optimal discrete-time admissible policy with time interval Δt. That is $V^*_{\Delta t}$ is the optimal performance obtained without constraining to the functional form of Equation (3) or leveraging model calibration like Equation (5). Define $\theta^*_{\Delta t} := (\theta^*_{\phi,\Delta t}, \theta^*_{\pi,\Delta t}, \theta^*_{S,\Delta t}) \in \arg\max_{(\theta_\phi,\theta_\pi,\theta_S)\in\mathcal{A}} H(\theta_\phi, \theta_\pi, \theta_S)$ with the policy functional form of Equation (3), such that $V(\theta^*_{\Delta t})$ is the performance that FaLPO can achieve with infinite data and perfect optimization. Then, Theorem 4.1 shows that the gap between $V^*_{\Delta t}$ and $V(\theta^*_{\Delta t})$ converges to zero as Δt goes to zero.

Theorem 4.1. *With assumptions above,* $\lim_{\Delta t\to 0}\left(V^*_{\Delta t} - V(\theta^*_{\Delta t})\right) = 0$.

Theorem 4.1 justifies the methodology of FaLPO under a small time interval. Proof in Appendices I.2 and I.3.

4.2 Non-Asymptotic Analysis

We now study the finite-sample performance of FaLPO. In each iteration, we collect B independent trajectories to estimate the gradient of H. Let θ_n be the estimate after the nth iteration, and N the total number of iterations. We analyze the average estimate $\bar{\theta} := \frac{\sum_{n=1}^{N}\theta_n}{N}$ instead of θ_N, which is a common technique for stochastic optimization analysis. Specifically, we aim to bound the expected difference between $V^*_{\Delta t}$ and $V(\bar{\theta})$. Note that it is extremely challenging to theoretically analyze a non-convex stochastic optimization equation (5) without further specifications in problem setup and assumptions (Polyak, 1963; Bhandari & Russo, 2024; Jin et al., 2021; Ma, 2021; Wang et al., 2020). Therefore, we consider a projection-based variant of FaLPO, under which the optimization process is conducted in a bounded parameter set $\mathcal{B} \subseteq \mathcal{A}$. Furthermore, we assume that the objective function H is strongly concave in $\mathcal{B}$ with a local maximal point $\theta^\dagger_{\Delta t} := (\theta^\dagger_{\phi,\Delta t}, \theta^\dagger_{P,\Delta t}, \theta^\dagger_{S,\Delta t})$. Similar local curvature assumptions are commonly used to analyze non-convex problems (Bach et al., 2017; Loh, 2017). With the above setup and assumptions (also detailed in Appendix J.2), the expected gap between $V^*_{\Delta t}$ and $V(\bar{\theta})$ satisfies the following finite-sample bound in Theorem 4.2.

Theorem 4.2. *With the aforementioned projection-based FaLPO algorithm and assumptions, there exist positive constants C_1, C_2, C_3, and C_4 such that*

$$\begin{aligned}
&\mathbb{E}[V^*_{\Delta t} - V(\bar{\theta})] \\
&\leq \frac{e_{\Delta t}}{1-\lambda} + \frac{H(\theta^*_{\Delta t}) - H(\theta^\dagger)}{1-\lambda} + \frac{C_1\log(N)}{N(1-\lambda)} \\
&\quad + \frac{C_1\log(N)}{BN(1-\lambda)}\left[(1-\lambda)^2 C_2 + \lambda^2 C_3 + 2\lambda(1-\lambda)C_4\right],
\end{aligned} \tag{7}$$

where $\lambda \in [0,1]$, and $e_{\Delta t}$ is an error term not related to N or B but dependent on Δt with $\lim_{\Delta t\to 0} e_{\Delta t} = 0$.

Theorem 4.2 provides a non-asymptotic upperbound on the gap between the optimal performance $V^*_{\Delta t}$ and the one achieved by FaLPO $V(\bar{\theta})$. We briefly comment on each term in the upperbound. $\frac{e_{\Delta t}}{1-\lambda}$ bounds the asymptotic performance gap caused by leveraging the continuous-time policy functional form constraint and model calibration, and we explain its connection to Theorem 4.1 in Appendix J.4. $\frac{H(\theta^*_{\Delta t}) - H(\theta^\dagger_{\Delta t})}{1-\lambda}$ controls the performance gap between the local optimal point $\theta^\dagger_{\Delta t}$ and the global optimal point $\theta^*_{\Delta t}$. The remaining terms characterize the performance gap between $\bar{\theta}$ and $\theta^\dagger_{\Delta t}$.

Theorem 4.2 has two implications. First, the bound in Equation (7) is a rational function of λ. Accordingly, there exist situations where a $\lambda \in (0,1)$ results a smaller upper bound than $\lambda = 0$, indicating the possibility that tuning λ can provide better performance (see experiments in Appendix J). Second, when $\lambda = 1$, the bound diverges to infinity. This makes sense since when $\lambda = 1$, $H(\theta_\phi, \theta_\pi, \theta_S) = L(\theta_\phi, \theta_S)$ does not contain θ_π: the algorithm does not learn the policy. We prove the theorem in Appendices J.1, J.3 and J.4.

5 Experiments

By incorporating continuous-time finance models into policy learning, FaLPO can deal with high data noise and complex factor effects. In this section, we demonstrate the improved performance of FaLPO against existing portfolio optimization methods, over synthetic and real-world experiments.

5.1 Synthetic Experiments

Metrics We compare different methods using the average terminal utility since it is the ultimate goal in our portfolio optimization problem formulation and is commonly used in continuous-time finance models. There exist other statistics measuring the performance of portfolios (see Section B). These statistics are not equivalent or consistent with the utility, and thus we do not emphasize them.

Table 1: Competing methods and their characteristics.

Methods	Factor Representation	Parametric Modeling	Joint Optimization
MMMC	✖	✔	✖
DDPG	✔	✖	✖
SLAC	✔	✖	✔
RichID	✔	✔	✖
CT-MB-RL	✖	✔	✖
FaLPO	✔	✔	✔

Methods FaLPO combines 1) flexible factor representation learning, 2) parametric modeling, and 3) joint optimization of policy learning and model calibration. To demonstrate the performance improvement of the combination of these three features, we compare FaLPO with five competing methods in prior work (Table 1). (i) *Merton Model with Model Calibration (MMMC)*: model calibration of a classic continuous-time finance baseline, which does not consider stochastic factors (Merton, 1969). (ii) *Deep Deterministic Policy Gradient (DDPG)*: a state-of-the-art model-free RL method with deterministic policy (Silver et al., 2014), which is at the core of many empirical portfolio optimization methods (Appendix A). DDPG directly treats factors as input of neural networks for policy without parametric modeling and joint optimization. (iii) *Stochastic latent actor critic (SLAC)*: a state-of-the-art representation learning RL method that jointly learns the policy and the representation of variables (a.k.a factors in our case) (Lee et al., 2020). But SLAC does not use any parametric models in representation learning or policy learning. (iv) *Model-based RL with rich observations (RichID)*: a state-of-the-art model-based RL method with representation learning (Mhammedi et al., 2020). RichID learns the representation of factors using parametric models, but it does not conduct a joint optimization on performance and model calibration like FaLPO. (v) *Continuous-time model-based RL (CT-MB-RL)*: model-based policy gradient where factors are fed into the policy functional derived from continuous-time models (Herzog et al., 2004) without representation learning. *Note that all the considered methods except MMMC observe the same data with stock prices S_t and factors Y_t.*

For policy gradient methods, we pick a deterministic policy approach like DDPG as, when compared to non-deterministic policy gradient alternatives, they are more suitable to portfolio optimization due to the continuous action space, high exploration cost, and high noise in financial data (Appendix A.2). For portfolio optimization, different variance reduction methods for policy gradient (Schulman et al., 2015; 2017; Xu et al., 2020) only provide minor performance improvements (Aboussalah et al., 2022). We hence do not report such results. For areas of RL with representation learning and model-based RL, we focus on those (SLAC and RichID) explicitly learning a representation of latent variables, since such methods are more closely related to FaLPO. There are other techniques like data augmentation, feature construction, adversarial training, and regularization that can improve the empirical performance of portfolio optimization (See Hambly et al. 2023 and Appendix A). In this work, we focus on the central methodological task of policy learning, and most such techniques can be directly combined with our proposed method.

Protocol We simulate environments with the Kim–Omberg model and implement the considered methods to compare their performance. Note that a key data generating parameter in portfolio optimization is the signal-to-noise ratio, which can be roughly characterized by the ratio between the scale of the drift and the scale of the volatility (see Appendix K.1 for detailed explanation). We test our method under different signal-to-noise ratios. To this end, we randomly generate stock drifts to around 10% (to mimic the real-world average return of stocks in SP500), vary the scale of volatility in $\{10\%, 20\%, 30\%\}$, and simulate data following the procedure in Appendix K.2. Then, we apply the considered methods to maximize the terminal power and

Table 2: Average terminal utility after tuning with standard deviation for synthetic data

Annual Volatility	0.1	0.2	0.3
FaLPO	$\mathbf{-0.465} \pm 0.446$	$\mathbf{-1.35} \pm 0.155$	$\mathbf{-2.737} \pm 0.219$
DDPG	-1.650 ± 0.456	-3.30 ± 1.294	-5.495 ± 1.269
SLAC	-0.750 ± 0.210	-5.50 ± 0.011	-6.160 ± 0.012
RichID	-3.350 ± 0.111	-5.65 ± 0.102	-6.325 ± 0.048
CT-MB-RL	-2.850 ± 0.014	-5.35 ± 0.020	-6.160 ± 0.026
MMMC	-4.723 ± 7.619	-5.602 ± 4.299	-6.124 ± 3.217

Table 3: Average terminal utility for real-world data. Mix denotes a mix of stocks in the previous three sectors.

Methods	Energy	Material	Industrials	Mix
FaLPO	$\mathbf{-2.4} \pm 1.9$	$\mathbf{-3.2} \pm 1.0$	$\mathbf{-6.3} \pm 2.3$	$\mathbf{-3.5} \pm 1.5$
DDPG	-6.6 ± 1.2	-7.3 ± 1.5	-7.3 ± 2.1	$-2.5 \times 10^4 \pm 3.3 \times 10^8$
SLAC	-6.8 ± 0.2	-7.0 ± 1.5	-342.4 ± 886.8	$-3.0 \times 10^8 \pm 4.3 \times 10^{12}$
RichID	-6.5 ± 0.1	-6.9 ± 1.4	-6.9 ± 0.4	-8.1 ± 3.9
CT-MB-RL	-4.2 ± 6.2	-5.4 ± 4.3	-11655 ± 32947.5	-5.7 ± 3.1
MMMC	-8.5 ± 7.6	-6.5 ± 1.7	-11.0 ± 5.4	-7.5 ± 4.4

exponential utility with different γ's. For each method, we tune the learning rate and other method-specific hyperparameters with early stopping (Appendix K.3). With each method-hyperparameter-environment combination, we repeat training, validation, and testing five times.

Results For exponential utility maximization, Table 2 summarizes the average test utility after hyperparameter selection with 10 stocks, 10 factors, and $\gamma = 5$. FaLPO outperforms all the competing methods in terms of average terminal utility. This performance gain may be explained by the factor representation learning informed by the continuous-time finance model, as other methods are incapable of doing so. Meanwhile, MMMC and CT-MB-RL underperform, which suggests the disadvantage of using oversimplified models. Compared with the more sophisticated RL methods like SLAC and RichID, the simple DDPG is fairly competitive. This is consistent with the existing observation that more complicated RL solutions may not always be suitable for portfolio optimization due to the large noise and idiosyncrasy in the data. In the appendix, we provide additional experimental results with different problem dimensions (Appendix K.4.1), other γ values (Appendix K.4.2), and different utility functions (Appendix K.4.3). The results are consistent. Appendix K.4.4 studies a simplified case, where the optimal performance can be mathematically derived. FaLPO achieves a similar performance as the theoretically optimal one.

5.2 Real-World Stock Trading

In this section, we present an application of FaLPO to real-world stock trading problems. Following the synthetic portfolio optimization setup, we study the six considered methods for 21-days (one month) stock trading in four different stock sectors using the daily stock price data from Yahoo finance between January 4, 2006 and April 1, 2022. For factors, we follow existing works (Aboussalah et al., 2022; De Prado, 2018; Dixon et al., 2020) and consider economic indexes, technical analysis indexes, and sector-specific factors such as oil prices, gold prices, and related ETF prices, leading to around 30 factors for each sector. In each sector we select 10 stocks according to the availability and trading volume in the considered time range (Appendix L.1). The training, validation, and testing data are constructed using rolling windows (Appendix L.3). Table 3 reports the achieved average utility of each method under the selected hyperparamters. FaLPO achieves the highest average utility in all four sectors.

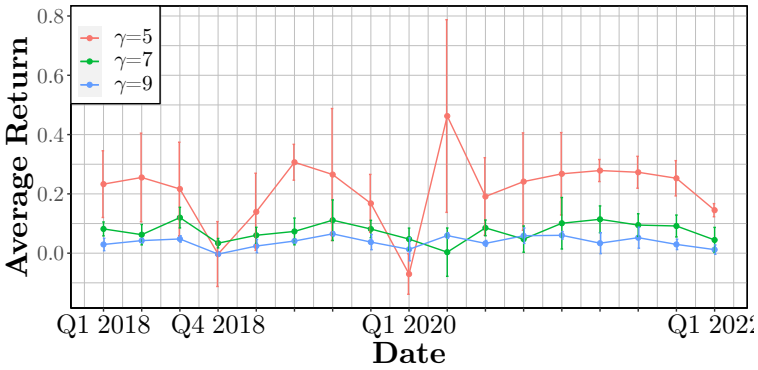

Figure 4: FaLPO average return over portfolio terminal dates.

Next, we conduct the training-tuning-testing procedure above with $\gamma \in \{5, 7, 9\}$, and report the returns of FaLPO in each quarter in Figure 4. Recall that a smaller γ corresponds to taking more risk. This is consistent with the observation in Figure 4 that the smaller the γ the bigger the return but the larger the fluctuations. Also, the return fluctuates and drops around late 2018 and early 2020. The former corresponds to the abrupt bear market at the end of 2018, and the latter is consistent with the time period that COVID-19 bursts. Under these two time periods, the financial market was especially noisy and unpredictable. In Appendices L.6 to L.8, we conduct additional experiments to further demonstrate the characteristics of FaLPO under various scenarios including discussions on transaction costs, sensitivity analysis, and different initial wealth First, we provide experimental results with short-selling transaction costs in Appendix L.6. This is in contrast to many existing works of utility maximization (Merton, 1969; Kim & Omberg, 1996; Avanesyan, 2021; Guan & Liu, 2021), which do not consider transaction costs even with shorting. We also believe that further studying other market frictions is an interesting direction for future work. Second, we implement sensitivity analysis on λ in Appendix L.4 and observe that a non-zero small λ works well in practice. Then, we compare different methods using Sharpe ratio and largest drawdon in Appendix L.7. Finally, we experiment with different initial wealth values with results provided in Appendix L.8.

6 Conclusion and Future Work

This work proposes FaLPO, a new decision-making framework for portfolio optimization with stochastic factors. By using continuous-time finance models to regularize policy learning, FaLPO is able to handle high noise and complex effects in financial data.

FaLPO has two potential limitations. First, while we show the extension of FaLPO to problems beyond portfolio optimization, FaLPO is not applicable when there is no suitable parametric model. Second, the performance of FaLPO still relies on good factors (Y_t). In the presence of unpredictable market events (like COVID-19), or when the factors do not contain any useful signals (like the Merton case in Appendix K.4.4), additional caution needs to be taken.

Future work includes applying FaLPO to other areas like paycheck optimization (Alaluf et al., 2023), circuit design (Mina et al., 2023), disease treatment (Geng et al., 2019a), and diagnosis (Geng et al., 2018; 2019b; Kuusisto et al., 2013). And leveraging other learners for the policy function (Li et al., 2024; Hazimeh et al., 2020; Gorishniy et al., 2021).

References

Amine Mohamed Aboussalah, Ziyun Xu, and Chi-Guhn Lee. What is the value of the cross-sectional approach to deep reinforcement learning? *Quantitative Finance*, 22(6):1091–1111, 2022.

Alekh Agarwal, Sham M Kakade, Jason D Lee, and Gaurav Mahajan. On the theory of policy gradient methods: Optimality, approximation, and distribution shift. *Journal of Machine Learning Research*, 22

(98):1–76, 2021.

Yacine Aït-Sahalia. Closed-form likelihood expansions for multivariate diffusions. *The Annals of Statistics*, 36(2):906–937, 2008.

Yacine Aït-Sahalia and Robert L. Kimmel. Estimating affine multifactor term structure models using closed-form likelihood expansions. *Journal of Financial Economics*, 98(1):113–144, 2010.

Melda Alaluf, Giulia Crippa, Sinong Geng, Zijian Jing, Nikhil Krishnan, Sanjeev Kulkarni, Wyatt Navarro, Ronnie Sircar, and Jonathan Tang. Reinforcement learning paycheck optimization for multivariate financial goals. *Risk and Decision Analysis*, 9(1):11–18, 2023.

Levon Avanesyan. *Optimal Investment in Incomplete Markets with Multiple Brownian Externalities*. PhD thesis, Princeton University, 2021.

Levon Avanesyan, Mykhaylo Shkolnikov, and Ronnie Sircar. Construction of forward performance processes in stochastic factor models and an extension of Widder's theorem. *Finance and Stochastics*, 24(4):981–1011, 2020.

Stephen H Bach, Bryan He, Alexander Ratner, and Christopher Ré. Learning the structure of generative models without labeled data. In *International Conference on Machine Learning*, pp. 273–282, 2017.

Krzysztof Bartoszek, Sylvain Glémin, Ingemar Kaj, and Martin Lascoux. Using the Ornstein–Uhlenbeck process to model the evolution of interacting populations. *Journal of Theoretical Biology*, 429:35–45, 2017.

Maximilian Behr, Peter Benner, and Jan Heiland. Invariant Galerkin Ansatz spaces and Davison-Maki methods for the numerical solution of differential Riccati equations. *Applied Mathematics and Computation*, 410:126401, 2021.

Yoshua Bengio. Using a financial training criterion rather than a prediction criterion. *International Journal of Neural Systems*, 8(4):433–443, 1997.

Alexandros Beskos and Gareth O. Roberts. Exact simulation of diffusions. *The Annals of Applied Probability*, 15(4):2422–2444, 2005.

Jalaj Bhandari and Daniel Russo. Global optimality guarantees for policy gradient methods. *Operations Research*, 72(5):1906–1927, 2024.

Homanga Bharadhwaj, Mohammad Babaeizadeh, Dumitru Erhan, and Sergey Levine. INFOrmation Prioritization through EmPOWERment in Visual Model-Based RL. In *International Conference on Learning Representations*, 2022.

Lukas Biewald. Experiment tracking with weights and biases, 2020. URL `https://www.wandb.com/`. Software available from wandb.com.

Jaya P. N. Bishwal. *Parameter Estimation in Stochastic Differential Equations*. Springer, 2007.

Tomas Björk. *Arbitrage Theory in Continuous Time*. Oxford University Press, 2009.

Simone P Blomberg, Suren I Rathnayake, and Cheyenne M Moreau. Beyond brownian motion and the Ornstein–Uhlenbeck process: Stochastic diffusion models for the evolution of quantitative characters. *The American Naturalist*, 195(2):145–165, 2020.

George Chacko and Luis M Viceira. Dynamic consumption and portfolio choice with stochastic volatility in incomplete markets. *The Review of Financial Studies*, 18(4):1369–1402, 2005.

Yevgen Chebotar, Karol Hausman, Marvin Zhang, Gaurav Sukhatme, Stefan Schaal, and Sergey Levine. Combining model-based and model-free updates for trajectory-centric reinforcement learning. In *International Conference on Machine Learning*, pp. 703–711, 2017a.

Yevgen Chebotar, Mrinal Kalakrishnan, Ali Yahya, Adrian Li, Stefan Schaal, and Sergey Levine. Path integral guided policy search. In *International Conference on Robotics and Automation*, pp. 3381–3388, 2017b.

Marco Corazza and Francesco Bertoluzzo. Q-learning-based financial trading systems with applications. Technical report, University Ca'Foscari of Venice, Dept. of Economics, 2014.

Marcos Lopez De Prado. *Advances in Financial Machine Learning*. John Wiley & Sons, 2018.

Marc Deisenroth and Carl E Rasmussen. PILCO: A model-based and data-efficient approach to policy search. In *International Conference on Machine Learning*, pp. 465–472, 2011.

Matthew F Dixon, Igor Halperin, and Paul Bilokon. *Machine Learning in Finance*. Springer, 2020.

Kenji Doya. Reinforcement learning in continuous time and space. *Neural Computation*, 12(1):219–245, 2000.

Benjamin Eysenbach, Alexander Khazatsky, Sergey Levine, and Russ R Salakhutdinov. Mismatched no more: Joint model-policy optimization for model-based RL. In *Advances in Neural Information Processing Systems*, volume 35, pp. 23230–23243, 2022.

Eugene F Fama and Kenneth R French. The cross-section of expected stock returns. *The Journal of Finance*, 47(2):427–465, 1992.

Eugene F Fama and Kenneth R French. A five-factor asset pricing model. *Journal of Financial Economics*, 116(1):1–22, 2015.

Vicky Fasen. Statistical estimation of multivariate Ornstein–Uhlenbeck processes and applications to co-integration. *Journal of Econometrics*, 172(2):325–337, 2013.

Damir Filipović and Eberhard Mayerhofer. *Affine Diffusion Processes: Theory and Applications*, pp. 125–164. De Gruyter, 2009.

Wendell Fleming and Raymond Rishel. *Deterministic and Stochastic Optimal Control*. Springer, 1975.

Wendell H Fleming and Sanjoy K Mitter. Optimal control and nonlinear filtering for nondegenerate diffusion processes. *Stochastics: An International Journal of Probability and Stochastic Processes*, 8(1):63–77, 1982.

Wendell H Fleming and Halil Mete Soner. *Controlled Markov Processes and Viscosity Solutions*. Springer, 2006.

Jean-Pierre Fouque, Ronnie Sircar, and Thaleia Zariphopoulou. Portfolio optimization and stochastic volatility asymptotics. *Mathematical Finance*, 27(3):704–745, 2017.

S Geng, Z Kuang, P. L. Peissig, D Page, L Maursetter, and K. E. Hansen. Parathyroid hormone independently predicts fracture, vascular events, and death in patients with stage 3 and 4 chronic kidney disease. *Osteoporosis International*, 30:2019–2025, 2019a.

Sinong Geng, Zhaobin Kuang, Peggy Peissig, and David Page. Temporal poisson square root graphical models. In *International Conference on Machine Learning*, pp. 1714–1723, 2018.

Sinong Geng, Minhao Yan, Mladen Kolar, and Sanmi Koyejo. Partially linear additive gaussian graphical models. In *International Conference on Machine Learning*, pp. 2180–2190, 2019b.

Sinong Geng, Houssam Nassif, Carlos Manzanares, Max Reppen, and Ronnie Sircar. Deep PQR: Solving inverse reinforcement learning using anchor actions. In *International Conference on Machine Learning*, pp. 3431–3441, 2020.

Sinong Geng, Houssam Nassif, and Carlos A. Manzanares. A data-driven state aggregation approach for dynamic discrete choice models. In *Uncertainty in Artificial Intelligence (UAI)*, pp. 647–657, 2023.

Sinong Geng, Aldo Pacchiano, Andrey Kolobov, and Ching-An Cheng. Improving offline RL by blending heuristics. In *International Conference on Learning Representations*, 2024.

Mohammad Ghavamzadeh, Shie Mannor, Joelle Pineau, Aviv Tamar, et al. Bayesian reinforcement learning: A survey. *Foundations and Trends® in Machine Learning*, 8(5–6):359–483, 2015.

Xavier Glorot and Yoshua Bengio. Understanding the difficulty of training deep feedforward neural networks. In *International Conference on Artificial Intelligence and Statistics*, pp. 249–256, 2010.

Yury Gorishniy, Ivan Rubachev, Valentin Khrulkov, and Artem Babenko. Revisiting deep learning models for tabular data. *Advances in Neural Information Processing Systems*, 34:18932–18943, 2021.

Amit Goyal and Pedro Santa-Clara. Idiosyncratic risk matters! *The Journal of Finance*, 58(3):975–1007, 2003.

Shixiang Gu, Timothy Lillicrap, Ilya Sutskever, and Sergey Levine. Continuous deep Q-learning with model-based acceleration. In *International Conference on Machine Learning*, pp. 2829–2838, 2016.

Mao Guan and Xiao-Yang Liu. Explainable deep reinforcement learning for portfolio management: An empirical approach. In *International Conference on AI in Finance*, pp. 1–9, 2021.

Tuomas Haarnoja, Aurick Zhou, Pieter Abbeel, and Sergey Levine. Soft actor-critic: Off-policy maximum entropy deep reinforcement learning with a stochastic actor. In *International Conference on Machine Learning*, pp. 1861–1870, 2018.

Danijar Hafner, Timothy Lillicrap, Ian Fischer, Ruben Villegas, David Ha, Honglak Lee, and James Davidson. Learning latent dynamics for planning from pixels. In *International Conference on Machine Learning*, pp. 2555–2565, 2019.

Ben Hambly, Renyuan Xu, and Huining Yang. Recent advances in reinforcement learning in finance. *Mathematical Finance*, 33:37–503, 2023.

Elad Hazan and Satyen Kale. Beyond the regret minimization barrier: An optimal algorithm for stochastic strongly-convex optimization. In *Conference on Learning Theory*, pp. 421–436, 2011.

Hussein Hazimeh, Natalia Ponomareva, Petros Mol, Zhenyu Tan, and Rahul Mazumder. The tree ensemble layer: Differentiability meets conditional computation. In *International Conference on Machine Learning*, pp. 4138–4148, 2020.

Florian Herzog, Gabriel Dondi, Hans P Geering, and Lorenz Schumann. Continuous-time multivariate strategic asset allocation. In *Annual Meeting of the German Finance Association*, pp. 1–34, 2004.

Desmond J Higham, Xuerong Mao, and Andrew M Stuart. Strong convergence of euler-type methods for nonlinear stochastic differential equations. *SIAM Journal on Numerical Analysis*, 40(3):1041–1063, 2002.

Vladimír Holý and Petra Tomanová. Estimation of Ornstein–Uhlenbeck process using ultra-high-frequency data with application to intraday pairs trading strategy. *arXiv preprint arXiv:1811.09312*, 2018.

Guosheng Hu, Yuxin Hu, Kai Yang, Zehao Yu, Flood Sung, Zhihong Zhang, Fei Xie, Jianguo Liu, Neil Robertson, Timpathy Hospedales, and Qiangwei Miemie. Deep stock representation learning: From candlestick charts to investment decisions. In *International Conference on Acoustics, Speech and Signal Processing*, pp. 2706–2710, 2018.

Michael Janner, Justin Fu, Marvin Zhang, and Sergey Levine. When to trust your model: Model-based policy optimization. *Advances in Neural Information Processing Systems*, 32, 2019.

Zhengyao Jiang, Dixing Xu, and Jinjun Liang. A deep reinforcement learning framework for the financial portfolio management problem. *arXiv preprint arXiv:1706.10059*, 2017.

Chi Jin, Praneeth Netrapalli, Rong Ge, Sham M Kakade, and Michael I Jordan. On nonconvex optimization for machine learning: Gradients, stochasticity, and saddle points. *Journal of the ACM*, 68(2):1–29, 2021.

Hilbert J Kappen. Path integrals and symmetry breaking for optimal control theory. *Journal of Statistical Mechanics: Theory and Experiment*, 2005(11):P11011, 2005.

Hilbert Johan Kappen and Hans Christian Ruiz. Adaptive importance sampling for control and inference. *Journal of Statistical Physics*, 162(5):1244–1266, 2016.

Ioannis Karatzas and Steven Shreve. *Brownian Motion and Stochastic Calculus*. Springer, 1987.

Belhal Karimi, Blazej Miasojedow, Eric Moulines, and Hoi-To Wai. Non-asymptotic analysis of biased stochastic approximation scheme. In *Conference on Learning Theory*, pp. 1944–1974, 2019.

Taesup Kim, Sungjin Ahn, and Yoshua Bengio. Variational temporal abstraction. *Advances in Neural Information Processing Systems*, 32, 2019.

Tong Suk Kim and Edward Omberg. Dynamic nonmyopic portfolio behavior. *The Review of Financial Studies*, 9(1):141–161, 1996.

Holger Kraft. Optimal portfolios and Heston's stochastic volatility model: An explicit solution for power utility. *Quantitative Finance*, 5(3):303–313, 2005.

Finn Kuusisto, Inês Dutra, Houssam Nassif, Yirong Wu, Molly E Klein, Heather B Neuman, Jude Shavlik, and Elizabeth S Burnside. Using machine learning to identify benign cases with non-definitive biopsy. In *International Conference on E-Health Networking, Application & Services*, pp. 283–285, 2013.

Michael Laskin, Denis Yarats, Hao Liu, Kimin Lee, Albert Zhan, Kevin Lu, Catherine Cang, Lerrel Pinto, and Pieter Abbeel. URLB: Unsupervised reinforcement learning benchmark. In *Conference on Neural Information Processing Systems*, 2021.

Alex X Lee, Anusha Nagabandi, Pieter Abbeel, and Sergey Levine. Stochastic latent actor-critic: Deep reinforcement learning with a latent variable model. In *Advances in Neural Information Processing Systems*, volume 33, pp. 741–752, 2020.

Boyao Li, Alexander J Thomson, Houssam Nassif, Matthew M Engelhard, and David Page. On neural networks as infinite tree-structured probabilistic graphical models. *Advances in Neural Information Processing Systems*, 37:4598–4628, 2024.

Zhaoqi Li, Houssam Nassif, and Alex Luedtke. Estimation of subsidiary performance metrics under optimal policies. *Statistica Sinica*, 37(3), 2027.

Xiao-Yang Liu, Hongyang Yang, Jiechao Gao, and Christina Dan Wang. FinRL: Deep reinforcement learning framework to automate trading in quantitative finance. In *International Conference on AI in Finance*, pp. 1–9, 2021.

Po-Ling Loh. Statistical consistency and asymptotic normality for high-dimensional robust m-estimators. *The Annals of Statistics*, 45(2):866–896, 2017.

Tengyu Ma. *Why Do Local Methods Solve Nonconvex Problems?*, pp. 465–485. Cambridge University Press, 2021.

Sidra Mehtab and Jaydip Sen. A robust predictive model for stock price prediction using deep learning and natural language processing. In *International Conference on Business Analytics and Intelligence*, 2019.

Robert C Merton. Lifetime portfolio selection under uncertainty: The continuous-time case. *The Review of Economics and Statistics*, pp. 247–257, 1969.

Robert C Merton. *Continuous-Time Finance*. Blackwell, 1992.

Robert C Merton et al. An intertemporal capital asset pricing model. *Econometrica*, 41(5):867–887, 1973.

Zakaria Mhammedi, Dylan J Foster, Max Simchowitz, Dipendra Misra, Wen Sun, Akshay Krishnamurthy, Alexander Rakhlin, and John Langford. Learning the linear quadratic regulator from nonlinear observations. *Advances in Neural Information Processing Systems*, 33:14532–14543, 2020.

Rayan Mina, George E Sakr, and Houssam Nassif. Enhancing transistor sizing in analog IC design using a circuit-focused semi-supervised learning. In *International Multidisciplinary Conference on Engineering Technology*, pp. 223–228, 2023.

Johannes Muhle-Karbe, Max Reppen, and H. Mete Soner. A primer on portfolio choice with small transaction costs. *Annual Review of Financial Economics*, 9:301–331, 2017.

Rémi Munos. Policy gradient in continuous time. *Journal of Machine Learning Research*, 7:771–791, 2006.

Anusha Nagabandi, Gregory Kahn, Ronald S Fearing, and Sergey Levine. Neural network dynamics for model-based deep reinforcement learning with model-free fine-tuning. In *International Conference on Robotics and Automation*, pp. 7559–7566, 2018.

Abhishek Nan, Anandh Perumal, and Osmar R Zaiane. Sentiment and knowledge based algorithmic trading with deep reinforcement learning. In *International Conference on Database and Expert Systems Applications*, pp. 167–180, 2022.

Arkadi Nemirovski, Anatoli Juditsky, Guanghui Lan, and Alexander Shapiro. Robust stochastic approximation approach to stochastic programming. *SIAM Journal on Optimization*, 19(4):1574–1609, 2009.

Bernt Oksendal. *Stochastic Differential Equations: An Introduction with Applications*. Springer, 2013.

Matteo Papini, Damiano Binaghi, Giuseppe Canonaco, Matteo Pirotta, and Marcello Restelli. Stochastic variance-reduced policy gradient. In *International Conference on Machine Learning*, pp. 4026–4035, 2018.

P. C. B. Phillips. The structural estimation of a stochastic differential equation system. *Econometrica: Journal of the Econometric Society*, pp. 1021–1041, 1972.

Peter C. B. Phillips and Jun Yu. Maximum likelihood and gaussian estimation of continuous-time models in finance. In *Handbook of Financial Time Series*, pp. 497–530. Springer, 2009.

Boris T Polyak. Gradient methods for the minimisation of functionals. *USSR Computational Mathematics and Mathematical Physics*, 3(4):864–878, 1963.

Konrad Rawlik, Marc Toussaint, and Sethu Vijayakumar. On stochastic optimal control and reinforcement learning by approximate inference. In *International Joint Conference on Artificial Intelligence*, pp. 3052–3056, 2013.

A. Max Reppen and H. Mete Soner. Bias-variance trade-off and overlearning in dynamic decision problems. *arXiv preprint arXiv:2011.09349*, 2020.

Rori V Rohlfs, Patrick Harrigan, and Rasmus Nielsen. Modeling gene expression evolution with an extended Ornstein–Uhlenbeck process accounting for within-species variation. *Molecular Biology and Evolution*, 31 (1):201–211, 2014.

John Schulman, Sergey Levine, Pieter Abbeel, Michael Jordan, and Philipp Moritz. Trust region policy optimization. In *International Conference on Machine Learning*, pp. 1889–1897, 2015.

John Schulman, Filip Wolski, Prafulla Dhariwal, Alec Radford, and Oleg Klimov. Proximal policy optimization algorithms. *arXiv preprint arXiv:1707.06347*, 2017.

Shai Shalev-Shwartz, Yoram Singer, Nathan Srebro, and Andrew Cotter. Pegasos: Primal estimated sub-gradient solver for SVM. *Mathematical Programming*, 127(1):3–30, 2011.

David Silver, Guy Lever, Nicolas Heess, Thomas Degris, Daan Wierstra, and Martin Riedmiller. Deterministic policy gradient algorithms. In *International Conference on Machine Learning*, pp. 387–395, 2014.

Freek Stulp and Olivier Sigaud. Path integral policy improvement with covariance matrix adaptation. In *International Conference on Machine Learning*, pp. 1547–1554, 2012.

Jingrui Sun and Jiongmin Yong. *Stochastic Linear-Quadratic Optimal Control Theory: Open-Loop and Closed-Loop Solutions*. Springer Nature, 2020.

Richard S Sutton and Andrew G Barto. *Reinforcement Learning: An Introduction*. MIT Press, 2018.

Peter Tankov. *Financial Modelling with Jump Processes*. CRC Press, 2003.

Evangelos Theodorou, Jonas Buchli, and Stefan Schaal. A generalized path integral control approach to reinforcement learning. *The Journal of Machine Learning Research*, 11:3137–3181, 2010.

Brandon Trabucco, Xinyang Geng, Aviral Kumar, and Sergey Levine. Design-bench: Benchmarks for data-driven offline model-based optimization. In *International Conference on Machine Learning*, pp. 21677–21691, 2022.

Vladimir Vapnik. Principles of risk minimization for learning theory. In *Advances in Neural Information Processing Systems*, pp. 831–838, 1992.

Oldrich Vasicek. An equilibrium characterization of the term structure. *Journal of Financial Economics*, 5 (2):177–188, 1977.

J. von Neumann and O. Morgenstern. *Theory of Games and Economic Behavior*. Princeton University Press, 1947.

Jessica A Wachter. Portfolio and consumption decisions under mean-reverting returns: An exact solution for complete markets. *Journal of Financial and Quantitative Analysis*, 37(1):63–91, 2002.

Haoran Wang, Thaleia Zariphopoulou, and Xunyu Zhou. Exploration versus exploitation in reinforcement learning: A stochastic control approach. *arXiv preprint arXiv:1812.01552*, 2018.

Lingxiao Wang, Qi Cai, Zhuoran Yang, and Zhaoran Wang. Neural policy gradient methods: Global optimality and rates of convergence. In *International Conference on Learning Representations*, 2020.

Manuel Watter, Jost Springenberg, Joschka Boedecker, and Martin Riedmiller. Embed to control: A locally linear latent dynamics model for control from raw images. *Advances in Neural Information Processing Systems*, 28:2746–2754, 2015.

Ivo Welch and Amit Goyal. A comprehensive look at the empirical performance of equity premium prediction. *The Review of Financial Studies*, 21(4):1455–1508, 2008.

Zhuoran Xiong, Xiao-Yang Liu, Shan Zhong, Hongyang Yang, and Anwar Walid. Practical deep reinforcement learning approach for stock trading. In *Neural Information Processing Systems Workshops*, 2018.

Pan Xu, Felicia Gao, and Quanquan Gu. An improved convergence analysis of stochastic variance-reduced policy gradient. In *Uncertainty in Artificial Intelligence*, pp. 541–551. PMLR, 2020.

Jiongmin Yong and Xun Yu Zhou. *Stochastic Controls: Hamiltonian Systems and HJB Equations*. Springer, 1999.

Pengqian Yu, Joon Sern Lee, Ilya Kulyatin, Zekun Shi, and Sakyasingha Dasgupta. Model-based deep reinforcement learning for dynamic portfolio optimization. In *International Conference on Machine Learning Workshops*, 2019.

Thaleia Zariphopoulou. A solution approach to valuation with unhedgeable risks. *Finance and Stochastics*, 5 (1):61–82, 2001.

Appendix

A Related Literature

In this section, we discuss related literature.

A.1 Continuous-Time Finance Models

Existing strategies for solving portfolio optimization using continuous-time finance models can be loosely summarized as performing three steps:

1. Choosing the model for the dynamics, i.e. the type of stochastic differential equation (SDE).
2. Estimating the parameter of the selected model (which is also referred to as model fitting, model identification, or calibration).
3. Solving for the optimal policy under the estimated model. This step leverages stochastic optimal control tools (Fleming & Rishel, 1975; Fleming & Mitter, 1982; Fleming & Soner, 2006; Yong & Zhou, 1999).

Finding and estimating an appropriate model for stochastic optimal control requires significant domain knowledge. For instance, in finance, the modeler must specify both which factors are relevant and how they affect stock prices (Fama & French, 1992). Unless every relevant factor is correctly specified, optimal control can hardly lead to good performances. As a result, in stock trading, control methods require hand picking three to five economic indices as the factors, and assuming they follow a simple (often linear) SDE. Trading can benefit from much richer datasets including related option prices, technical indicators, and interest rates (Aboussalah et al., 2022; De Prado, 2018; Dixon et al., 2020; Mehtab & Sen, 2019).

Further, even with a correctly specified model and factors, likelihood-based estimation for SDE control models can be very challenging (Phillips & Yu, 2009). As a result, methods like Aït-Sahalia (2008); Aït-Sahalia & Kimmel (2010) seek to replace the exact likelihood with other likelihood-based objective functions, while maintaining theoretical guarantees. However, the proposed objective function needs to be derived for each specific problem, and the derivation can be challenging. Other methods like Fasen (2013); Holý & Tomanová (2018) rely on more specific parametric or low-dimensional setups. To alleviate these issues, our framework extends the existing continuous-time finance models by allowing for a flexible and generalized definition of stochastic factor dynamics. Furthermore, we simultaneously conduct policy learning and model calibration in an RL manner, with a square-loss objective that avoids the calculation of an exact likelihood.

A.2 Reinforcement Learning

RL aims to conduct the aforementioned three steps by (i) relying more on data (ii) in an end-to-end fashion. Methods like model-free RL assume no parametric forms on the dynamics, and directly learn the optimal policy while explicitly learning the model (step 1) and estimating the parameters (step 2).

Discrete-Time Model-Free RL There exist many discrete-time model-free RL methods (Sutton & Barto, 2018). In this category, deep deterministic policy gradient (DDPG) is the most relevant one, and is empirically most widely used for portfolio optimization (Hambly et al., 2023). The reason is twofold. First, DDPG is a policy-gradient based method, and thus can naturally handle continuous states and actions in portfolio optimization with simple procedures. Second, DDPG learns a deterministic policy instead of a stochastic one like Haarnoja et al. (2018). This characteristic is especially important in portfolio optimization where the policy learning goal is a deterministic policy since the cost of a stochastic policy is extremely expensive.

Continuous-Time Model-Free RL Continuous-time model-free RL (Wang et al., 2018; Doya, 2000; Munos, 2006) aims to solve for a continuous-time policy. However, such methods do not use or assume any SDE structure, and thus struggle with the common open questions in model-free RL like poor stability

and sample complexity. As an example, path integral methods stem from the theoretical result that the value function of a type of continuous-time decision-making problems can be expressed in closed form as a Feyman-Kac path integral (Fleming & Rishel, 1975; Kappen, 2005). A series of control/RL methods follow the rationale of optimizing the policy to maximize such an integral. Specifically, Theodorou et al. (2010) propose an open-loop control strategy; Kappen & Ruiz (2016) build RL with importance sampling; and Chebotar et al. (2017a;b); Stulp & Sigaud (2012) combine path integral with other model-based or model-free RL methods. However, the core derivation only holds for decision-making satisfying Kappen & Ruiz (2016, Equation (1)), which is equivalent to assuming that the action does not affect the randomness in decision-making. Such an assumption is limiting, and does not hold for portfolio optimization, where how to allocate the wealth in order to minimize the risk is key to a successful policy.

Model-based RL and RL with Representation Learning Model-based RL and RL with representation learning are two active research areas but without a clear general state-of-the-art (Bharadhwaj et al., 2022; Eysenbach et al., 2022; Trabucco et al., 2022; Janner et al., 2019; Deisenroth & Rasmussen, 2011; Nagabandi et al., 2018; Laskin et al., 2021; Lee et al., 2020; Watter et al., 2015; Chebotar et al., 2017a; Hafner et al., 2019; Kim et al., 2019). The closest to FaLPO are those that learn an explicit representation of a latent variable like Lee et al. (2020); Mhammedi et al. (2020). But such methods are unable to leverage continuous-time finance models for portfolio optimization.

Bayesian RL Our proposed framework is also related to Bayesian models (Ghavamzadeh et al., 2015; Rawlik et al., 2013), if we treat the learned representation of factors as the hidden variable. Strictly formulating an NSFM as a Bayesian model requires assumptions specifying the conditional distributions, and thus requires more domain knowledge. The optimization of Bayesian methods is also more challenging.

RL for Stock Trading Various authors applied RL to stock trading (Corazza & Bertoluzzo, 2014; Hambly et al., 2023; Nan et al., 2022; Xiong et al., 2018; Guan & Liu, 2021; Liu et al., 2021; Hu et al., 2018; Yu et al., 2019). However, these methods focus more on feature selection or empirical performance-improving techniques. Methodologically, they do not take advantage of continuous-time finance models.

A.3 Empirical Risk Minimization

Another related area is Empirical Risk Minimization (ERM) (Vapnik, 1992). ERM studies the minimization of an objective function using the averages over training data to construct an empirical loss function. Recent work connected ERM with simulation-based and data-based offline decision-making methods (Reppen & Soner, 2020). More specifically, when the random input is observable and unaffected by actions, and a training set is available, the decision-making problem can be formulated as an ERM problem. As a result, the portfolio optimization may be reformulated as an ERM extension.

B Other Objective Functions

The goal of portfolio optimization is to maximize the return while minimizing or constraining the risk. In practice, one can use different objective functions for such a goal, like mean-variance (Hambly et al., 2023), Sharpe ratio, and so on. In this work, we consider utility maximization with power utility and exponential utility. The proposed method also works with other objective functions, as long as we can derive (part of) the optimal policy structure. The selection among these objective functions is a user-preference question. We note that, in principle, one could also combine multiple objective functions into a composite loss (Li et al., 2027); however, we do not explore this direction in the present work.

C Gradient Estimates

In this section, we discuss the gradient estimation for both V and L. Assume that we collect B independent trajectories for S_t and Y_t, denoted as

$$\mathbb{D} := \{(s_{0,k}, y_{0,k}), (s_{\Delta t,k}, y_{\Delta t,k}), (s_{2\Delta t,k}, y_{2\Delta t,k}), \cdots (s_{M\Delta t,k}, y_{M\Delta t,k})\}_{k=1}^{B}.$$

Then, the gradient estimate for $V(\theta_\phi, \theta_\pi)$ is defined as

$$\bar{\nabla} V(\theta_\phi, \theta_\pi) := \frac{1}{B} \sum_{k=1}^{B} \tilde{\nabla} V_k(\theta_\phi, \theta_\pi) \text{ with } \tilde{\nabla} V_k(\theta_\phi, \theta_\pi) := \nabla_{\theta_\phi, \theta_\pi} U(z_{T,k}^{\pi(\cdot;\theta_\phi,\theta_\pi),\Delta t}).$$

Let $z_{T,k}^{\pi(\cdot;\theta_\pi),\Delta t}$ denote the terminal wealth in trajectory k under policy $\pi(\cdot;\theta_\pi)$:

$$z_{T,k}^{\pi(\cdot;\theta_\pi),\Delta t} := z_0 + \sum_{m=1}^{M} z_{m-1} \left[\sum_{i=1}^{d_S} \pi^i(m\Delta t, y_{m\Delta t}; \theta_\phi, \theta_\pi) \frac{s^i_{(m+1)\Delta t} - s^i_{m\Delta t}}{s^i_{m\Delta t}} \right].$$

Next, we consider the gradient of L:

$$\bar{\nabla} L(\theta_\phi, \theta_S) := \frac{1}{B} \sum_{k=1}^{B} \tilde{\nabla} L_k(\theta_\phi, \theta_S).$$

Specifically for likelihood and negative mean square loss, we have

$$\begin{aligned} \tilde{\nabla} L_{Likelihood,k}(\theta_\phi, \theta_S) := & \frac{1}{M} \sum_{m=0}^{M-1} \nabla_{\theta_\phi, \theta_S} \log(\mathrm{P}(s_{(m+1)\Delta t,k}, \phi(y_{(m+1)\Delta t,k}; \theta_\phi) \\ & \mid s_{m\Delta t,k}, \phi(y_{m\Delta t,k}; \theta_\phi); \theta_S)), \end{aligned}$$

$$\begin{aligned} \tilde{\nabla} L_{NMSL,k}(\theta_\phi, \theta_S) := & -\frac{1}{M} \sum_{m=0}^{M-1} \sum_{i=1}^{d_S} \nabla_{\theta_\phi, \theta_S} \Bigg(\log(s^i_{(m+1)\Delta t,k}) - \log(s^i_{m\Delta t,k}) \\ & - \mathbb{E}\Bigg[\int_{m\Delta t}^{(m+1)\Delta t} f_S^j(X_s; \theta_S) \\ & - \frac{1}{2} \sum_{i=1}^{d_S} (g_S^{ij}(X_s; \theta_S))^2 ds \Bigg| s_{m\Delta t,k}, \phi(y_{m\Delta t,k}; \theta_\phi) \Bigg] \Bigg)^2. \end{aligned}$$

As a result, in each iteration, we collect B trajectories to estimate the gradient of $H(\theta_\phi, \theta_\pi)$.

D A Primer on Stochastic Differential Equations (SDEs)

We provide a general formulation of SDEs with two examples.

D.1 Formulation of SDEs

SDEs are a generalization of ordinary differential equations to dynamic systems influenced by random fluctuations. The structure of the randomness can in principle be quite general, such as with jump processes where the state evolution is no longer continuous (Tankov, 2003). Although our method can be generalized to all SDEs, we restrict ourselves to practical settings where the source of randomness is a Brownian motion.

Let W_t be a multi-dimensional independent standard Brownian motion. For a random process S_t, an SDE is typically expressed using a differential form as

$$dS_t = f(S_t)\, dt + g(S_t)\, dW_t, \text{ or } S_t = S_0 + \int_0^t f(S_t)\, dt + \int_0^t g(S_t)\, dW_t, \tag{8}$$

where $f(\cdot)$ and $g(\cdot)$ are functions of S_t. The stochastic integral $\int_0^t g(S_t) dW_t$ is the accumulation of influence to the state due to the noise. We refer the reader to Karatzas & Shreve (1987) for details on the construction of stochastic integrals and SDE theory. Important here is that Equation (8) defines the transition of S_t in an infinitesimal time step. The drift coefficient $f(S_t)$ characterizes the deterministic part of the change of S_t, and the diffusion coefficient $g(S_t)$ models the randomness in the transition of S_t.

D.2 Examples

As concrete examples, we discuss two families of SDEs widely used in finance, economics, and biology: Geometric Brownian motion (GBM) and Ornstein–Uhlenbeck (OU) processes (Merton et al., 1973; Vasicek, 1977; Bartoszek et al., 2017; Blomberg et al., 2020; Rohlfs et al., 2014). The OU structure appears in both applications below, and the financial application uses GBM as a base, but extends it with OU drift coefficients. The two types of SDEs are given by

$$\text{GBM: } \frac{dS_t}{S_t} = \mu\, dt + \sigma\, dW_t, \qquad \text{OU: } dS_t = \mu S_t\, dt + \sigma\, dW_t,$$

where $\frac{d\mathbf{S}_t}{\mathbf{S}_t} := \left\{\frac{dS_{it}}{S_{it}}\right\}$ denotes the component-wise division of S_t, and the matrices μ and σ define the drift and diffusion coefficients. We refer the interested reader to Fleming & Soner (2006) for more information on these topics.

D.3 Itô's Formula

Itô's Formula is a fundamental analytical tool for SDEs, and crucial for their analysis. We only provide a simple version here, which is sufficient for our analysis. A more general and rigorous statement with assumptions and proof of Itô's formula and integral can be found in Karatzas & Shreve (1987, Theorem 3.3).

Lemma D.1 (Itô's Formula)**.** *Consider a twice differentiable function G, and S_t following*

$$dS_t = f(S_t)\, dt + g(S_t)\, dW_t.$$

Then, we have

$$dG(t, S_t) = \left\{\frac{\partial G}{\partial t} + \left(\frac{\partial G}{\partial S_t}\right)^\top f(S_t) + \frac{1}{2}\operatorname{Tr}\left[g(S_t)^\top \frac{\partial^2 G}{\partial S_t^2} g(S_t)\right]\right\} dt + \left(\frac{\partial G}{\partial S_t}\right)^\top g(S_t) dW_t.$$

Lemma D.2. *For a suitable bounded process S_t, the Itô integral $\int_0^t S_t dW_t$ satisfies:*

$$\mathbb{E}\left[\int_0^t S_t dW_t\right] = 0, \qquad \mathbb{E}\left[\left(\int_0^t S_t dW_t\right)^2\right] = \mathbb{E}\left[\int_0^t S_t^2 dt\right].$$

The latter is also referred to as Itô's isometry

E Model Calibration

We discuss two model calibration loss functions, log-likelihood and negative mean square loss.

E.1 Log-Likelihood

We can use log-likelihood as L for model calibration. The log-likelihood of SDEs is derived in a sequential manner. Specifically, for EQuation (2) the log-likelihood is derived as

$$L_{Log-Likelihood}(\theta_\phi, \theta_S) := \mathbb{E}[\log(\mathrm{P}_{\theta_S}(S_{t+\Delta t}, \phi(Y_{t+\Delta t}; \theta_\phi) \mid S_t, \phi(Y_t; \theta_\phi)))], \tag{9}$$

where P_{θ_S} denotes the conditional likelihood according to Equation (2) but with parameter θ_S instead of θ_S^*. In specific models, one can derive $\mathrm{P}_{\theta_S}(S_{t+\Delta t}, \phi(Y_{t+\Delta t}) \mid S_t, \phi(Y_t); \theta)$ (Phillips, 1972; Holý & Tomanová, 2018; Beskos & Roberts, 2005) or the approximation of it (Aït-Sahalia & Kimmel, 2010).

E.2 Negative Mean Square Loss

For the SDE system of Equation (2), one can also use a negative mean square loss (NMSL) as the calibration objective. To derive this loss function, we first derive the dynamics of log price by applying Itô's Formula

Lemma D.1 to Equation (2):

$$d\log(S_t^i) = f_S^i(X_t;\theta_S)dt - \frac{1}{2}\sum_{j=1}^{d_W}(g_S^{ij}(X_s;\theta_S)])^2dt + \sum_{j=1}^{d_W} g_S^{ij}(X_s;\theta_S)]dW_t^j. \tag{10}$$

Then, combined with Lemma D.2, under proper assumptions of Lemma D.2, we pose an expectation over both sides of the above equation, and derive

$$\mathbb{E}[d\log(S_t^i)] = f_S^i(X_t;\theta_S)dt - \frac{1}{2}\sum_{j=1}^{d_W}(g_S^{ij}(X_s;\theta_S)])^2dt.$$

In words, the expectation of the log price change within an infinitesimal time is $f_S^i(X_t;\theta_S)dt - \frac{1}{2}\sum_{j=1}^{d_W}(g_S^{ij}(X_s;\theta_S)])^2dt$. Therefore, one can estimate the parameter θ_S by minimizing the mean square loss between the log price change and the expected log price change:

$$\begin{aligned} L_{NMSL}(\theta_S) := -\mathbb{E}\Bigg[\sum_{i=1}^{d_S}\Bigg(\log(S_{t+\Delta t}^i) - \log(S_t^i) - \mathbb{E}\Bigg[\int_t^{t+\Delta t} f_S^i(X_s;\theta_S) \\ - \frac{1}{2}\sum_{j=1}^{d_W}(g_S^{ij}(X_s;\theta_S))^2ds\Bigg|S_t, X_t\Bigg]\Bigg)^2\Bigg]. \end{aligned} \tag{11}$$

It can be easily proved that the true data generating SDE parameter satisfies

$$\theta_S^* \in \arg\max L_{NMSL}(\theta_S).$$

Further, if we take $X_t = \phi(Y_t;\theta_\phi)$ and parameterize the objective as $L_{NMSL}(\theta_\phi,\theta_S) := -\mathbb{E}\Bigg[\sum_{i=1}^{d_S}\left[\log(S_{t+\Delta t}^i) - \log(S_t^i) - \phi^i(Y_t;\theta_\phi)\Delta t - \theta_S^i\right]^2\Bigg]$, we can prove

$$\theta_\phi^*, \theta_S^* \in \arg\max L_{NMSL}(\theta_\phi,\theta_S).$$

Note that in practice it can be very hard to calculate the expectation $\mathbb{E}\big[\int_t^{t+\Delta t} f_S^i(X_s;\theta_S) - \frac{1}{2}\sum_{j=1}^{d_W}(g_S^{ij}(X_s;\theta_S))^2ds\big|S_t, X_t\big]$. Therefore, when Δt is small, we replace the conditional expectation via $\mathbb{E}\big[f_S^i(X_S;\theta_S)\Delta t - \frac{1}{2}\sum_{j=1}^{d_W}(g_S^{ij}(X_S;\theta_S))^2\Delta t\Big|S_t, X_t\big]$. Accordingly the calibration objective is defined as

$$L_{NMSL}(\theta_S) \approx -\mathbb{E}\Bigg[\sum_{i=1}^{d_S}\Bigg(\log(S_{t+\Delta t}^i) - \log(S_t^i) - f_S^i(X_s;\theta_S)\Delta t + \frac{1}{2}\sum_{j=1}^{d_W}(g_S^{ij}(X_s;\theta_S))^2\Delta t\Bigg]\Bigg)^2\Bigg]. \tag{12}$$

E.3 Other Model Calibration Objective

Another potential model calibration objective following the same rationale as Equation (11) is

$$\begin{aligned} L_{NMSL-X}(\theta_\phi,\theta_S) := -\mathbb{E}\Bigg[\sum_{i=1}^{d_X}\Bigg(\phi(Y_{t+\Delta t};\theta_\phi)^i - \phi(Y_t;\theta_\phi)^i \\ - \mathbb{E}\Bigg[\int_t^{t+\Delta t} f_X^i(\phi(Y_s;\theta_\phi)^i;\theta_S)ds\Bigg|\phi(Y_t;\theta_\phi)^i\Bigg]\Bigg)^2\Bigg], \end{aligned}$$

which is derived using the conditional expectation of $X_{t+\Delta}$ given X_t. However, the true data-generating parameter $(\theta_\phi^*, \theta_S^*)$ is not a maximal point of L_{NMSL-X}. To more clearly see this, this loss function encourages the representation function ϕ to take a constant output so that X_t is constant over time with $f_X^i(X_s;\theta_S) = 0$, and $L_{NMSL-X}(\theta_\phi) = 0$. We also try this loss in experiments, and it leads to poor validation and test performances.

F Applications of FaLPO to Different Stochastic Factor Models in Continuous-Time Finance

FaLPO can be used with many stochastic factor models in continuous-time finance models. In this section, we discuss the Merton model (Appendix F.1), Kim–Omberg (Appendix F.2) and EVE (Appendix F.3). These models differ in how factors influence asset price dynamics. In the Merton model, factors have no effect; in the Kim–Omberg model, factors affect only the drift; and in the EVE model, factors influence both drift and volatility. Choosing the appropriate model depends on the role of factors in driving price behavior. For instance, if asset prices are uncorrelated with the factors, the Merton model may be sufficient. If there is evidence that volatility also depends on the factors, then the EVE model may be more appropriate.

F.1 Merton Model

Merton model (Merton, 1969) is a classic setup for portfolio optimization. It studies the allocation of capital across a set of financial assets in order to maximize profits and minimize risks.

F.1.1 Modeling

Consider p risky assets with prices $S_t = \{S_t^i\}_{i=1}^p$ and an additional risk-free money market account with, for simplicity, zero interest rate of return (like cash). The Merton model does not include factors. The dynamics for asset prices is formulated as

$$\frac{dS_t^i}{S_t^i} = \mu\, dt + \sigma dW_t. \tag{13}$$

The parameters μ, σ are $p \times p$ matrices, with σ denoting the volatility of assets. Further, we use $\tilde{Z}_t^{\tilde{\pi}}$ to denote the wealth at time point t under the continuous-time policy $\tilde{\pi}$. Under the famous and widely used self-financing assumption (Björk, 2009), we have

$$\frac{d\tilde{Z}_t^{\tilde{\pi}}}{\tilde{Z}_t^{\tilde{\pi}}} = \tilde{\pi}_t \mu dt + \tilde{\pi}_t \sigma dW_t.$$

An investor's goal is to maximize the expected utility of capital $U(Z_T)$ at some future time point T:

$$\max_{\tilde{\pi}_t} \mathbb{E}_{\tilde{\pi}_t} \left[U(\tilde{Z}_T^{\tilde{\pi}}) | Z_0 = z, S_0 = s \right]. \tag{14}$$

Negative values in the policy output are allowed, meaning the agent can short any asset.

F.1.2 Policy Functional Form

For the Merton model, policy Π in Equation (3) can be explicitly derived.

Lemma F.1 (Policy Functional Form for Merton Model)**.** *For a Merton model defined in Equation* (13)*, under common assumptions, the optimal policy for portfolio optimization* (14) *with power utility is*

$$\tilde{\pi}^* = \mu(\sigma\sigma^\top)^{-1}.$$

The optimal policy for portfolio optimization (14) *with exponential utility is*

$$\tilde{\pi}^* = \frac{\mu(\sigma\sigma^\top)^{-1}}{\tilde{Z}_t^{\tilde{\pi}^*}}.$$

Proof. Lemma F.1 is a classic result in continuous-time finance, proposed in Merton (1969). □

In words, in a Merton model, the optimal policy is independent of time, stock prices, and factors. The optimal investment strategy is to keep a constant fraction or amount of wealth in each asset all along, depending on

the choice of utility function. Let θ_π be a $d_S \times 1$ parameter vector. According to Lemma F.1, in FaLPO, we parameterize the candidate policy function for power utility as

$$\pi(t, S_t, Z_t, Y_t; \theta_\phi, \theta_\pi) = \Pi(t, S_t, Z_t, \phi(Y_t; \theta_\phi); \theta_\pi) = \theta_\pi,$$

and for exponential utility as

$$\pi(t, S_t, Z_t, Y_t; \theta_\phi, \theta_\pi) = \Pi(t, S_t, Z_t, \phi(Y_t; \theta_\phi); \theta_\pi) = \frac{\theta_\pi}{Z_t}.$$

F.1.3 Model Calibration

According to the Merton model formulation, there exist no factors affecting the evolution of stock prices. Therefore, we do not add the model calibration objective in FaLPO for Merton problems.

F.2 Kim–Omberg Model

Kim–Omberg model (Kim & Omberg, 1996) is a standard model for portfolio optimization with predictable asset returns, extensively discussed in literature (Welch & Goyal, 2008; Muhle-Karbe et al., 2017).

F.2.1 Modeling

In Kim–Omberg model, the stock dynamics are formulated as

$$\begin{aligned} \frac{dS_t^i}{S_t^i} &= X_t^i \, dt + \sum_{j=1}^{d_W} \sigma^{ij} \, dW_t^j \\ dX_t &= \mu(\omega - X_t) \, dt + v \, dW_t. \end{aligned}$$

The portfolio optimization goal is formulated as

$$\max_{\tilde{\pi}_t} \tilde{V}(\tilde{\pi}_t) \text{ with } \tilde{V}(\tilde{\pi}_t) := \mathbb{E}_{\tilde{\pi}_t}[U(\tilde{Z}_t^{\tilde{\pi}})|X_0 = x, Z_0 = z, S_0 = s]. \tag{15}$$

F.2.2 Policy Functional Form

An optimal policy function is derived in Lemma F.2.

Lemma F.2. *Under common assumptions in Kim & Omberg (1996); Herzog et al. (2004), an optimal policy functional form for Equation* (15) *with power utility is derived as*

$$\tilde{\pi}^* = \frac{1}{1-\gamma}(\sigma\sigma^\top)^{-1}\big[X_t + \sigma v^\top (k_3(t) X_t + k_2(t))\big],$$

where $k_2(t)$ and $k_3(t)$ satisfy

$$\begin{aligned} &\frac{dk_1(t)}{dt} + \frac{1}{2}\operatorname{Tr}\left\{v^\top (k_2(t)k_2(t)^\top + k_3(t))v\right\} + (\mu\omega)^\top k_2(t) - \frac{\gamma}{2(\gamma-1)}(k_2(t)^\top v v^\top k_2(t)) = 0, \\ &\frac{dk_2(t)}{dt} + k_3(t) v v^\top k_2(t) - \mu^\top k_2(t) + k_3(t)\mu\omega - \frac{\gamma}{\gamma-1}((\sigma\sigma^\top)^{-1}\sigma v k_2(t) + k_3(t) v v^\top k_2(t)) = 0, \\ &\frac{dk_3(t)}{dt} + k_3(t) v v^\top k_3(t) - k_3(t)\mu - \mu^\top k_3(t) \\ &\quad - \frac{\gamma}{\gamma-1}((\sigma\sigma^\top)^{-1} + (\sigma\sigma^\top)^{-1}\sigma v^\top k_3(t) + k_3(t) v \sigma^\top (\sigma\sigma^\top)^{-1} + k_3(t) v v^\top k_3(t)) = 0, \end{aligned}$$

with $k_1(T) = 0$, $k_2(T) = 0$, and $k_3(T) = 0$. Note that $k_1(t)$ is a scalar, $k_2(t)$ is a $d_S \times 1$ vector, and $k_3(t)$ is a $d_X \times d_X$. The ODE of $k_3(t)$ is the famous matrix Riccati equation (Appendix G).

Similarly, an optimal policy functional form for Equation (15) *with exponential utility is derived as*

$$\tilde{\pi}_t^* = (\sigma\sigma^\top)^{-1}\frac{1}{-\gamma^2 Z_t}\Big[X(t) + \sigma v^\top(k_3(t)X_t + k_2(t))\Big],$$

where $k_2(t)$ *and* $k_3(t)$ *satisfy*

$$\begin{aligned}
&\frac{dk_1(t)}{dt} + \frac{1}{2}\operatorname{Tr}\left\{v^\top(k_2(t)k_2(t)^\top + k_3(t))v\right\} + (\mu\omega)^\top k_2(t) - \frac{1}{2}(k_2(t)^\top vv^\top k_2(t)) = 0,\\
&\frac{dk_2(t)}{dt} + k_3(t)vv^\top k_2(t) - \mu k_2(t) + k_3(t)\mu\omega - ((\sigma\sigma^\top)^{-1}\sigma v k_2(t) + k_3(t)vv^\top k_2(t)) = 0,\\
&\frac{dk_3(t)}{dt} + k_3(t)vv^\top k_3(t) - k_3(t)\mu - \mu^\top k_3(t)\\
&\quad - ((\sigma\sigma^\top)^{-1} + (\sigma\sigma^\top)^{-1}\sigma v^\top k_3(t) + k_3(t)v\sigma^\top(\sigma\sigma^\top)^{-1} + k_3(t)vv^\top k_3(t)),
\end{aligned}$$

with $k_1(T) = 0$, $k_2(T) = 0$, *and* $k_3(T) = 0$.

F.2.3 Model Calibration

Following the derivation in Appendix E.2, the negative mean square loss for Kim–Omberg model can be derived as $L(\theta_\phi, \theta_S) := -\mathbb{E}\Big[\sum_{i=1}^{d_S}\big[\log(S^i_{t+\Delta t}) - \log(S^i_t) - \phi^i(Y_t;\theta_\phi)\Delta t - \theta^i_S\big]^2\Big]$, where in this case θ_S is a $d_S \times 1$ vector.

F.3 EVE Model with Stochastic Markovian Factors

We take EVE model (Avanesyan et al., 2020) with stochastic Markovian factors as another example.

F.3.1 Modeling

We first detail the modeling of EVE, which formulates the dynamics of asset prices by

$$\begin{aligned}
\frac{dS^i_t}{S^i_t} &= \mu_i(X_t;\theta_S)dt + \sum_{j=1}^{d_W}\sigma_{ji}(X_t;\theta_S)dW^j_t, \quad i = 1, 2, \cdots, d_S,\\
dX_t &= \big(M^\top X_t + \omega\big)dt + \kappa(X_t;\theta_S)^\top dB_t,\\
B_t &= \rho^\top W_t + A^\top W^\perp_t.
\end{aligned} \tag{16}$$

We use W_t and $W^\perp_t$ to denote two sets of independent Brownian motions. ρ denotes a correlation matrix with components $\rho^{ij} \in [-1, 1]$. Therefore, B is indeed another Brownian motion. We let μ, σ, and κ be parametric functions, with θ_S denoting all the parameters. The SDE parameters include all the parameter matrices and $\boldsymbol{\beta}$'s. Again, with Z_t as the wealth, we aim to maximize the power utility at the terminal time $T > 0$ as the performance objective:

$$\tilde{V}(\tilde{\pi}_t) = \mathbb{E}_{\tilde{\pi}}\left[\frac{(\tilde{Z}^{\tilde{\pi}}_T)^{1-\gamma}}{1-\gamma}\right].$$

EVE model poses further assumptions on dynamics (16).

Assumption F.3. M has non-negative off-diagonal entries and $\omega \in [0, \infty)^k$. Further, we assume that there exist $\lambda(x)$, Λ and L, and N such that $\mu(\cdot)$, $\sigma(\cdot)$, $\kappa(\cdot)$ and ρ satisfy

$$\begin{aligned}
&\lambda(x)^\top\lambda(x) = \mu(x)^\top\sigma(x)^{-1}\big(\sigma(x)^{-1}\big)^\top\mu(x) = \Lambda^\top x\\
&\kappa(x)^\top\kappa(x) = diag(L_1x_1, L_2x_2, \cdots, L_kx_k), \text{ with } L_1, L_2, \cdots, L_k \geq 0\\
&\Gamma\kappa(x)^\top\rho^\top\lambda(x) = N^\top x.
\end{aligned} \tag{17}$$

The conditions in Assumption F.3 are necessary for the process of X_t to be $[0,\infty)^k$-valued and affine. Under these conditions, SDE (16) has a unique weak solution which is affine and takes values in $[0,\infty)^k$ (Filipović & Mayerhofer, 2009). Further, the EVE model requires the following two assumptions:

Assumption F.4 (Assumption 2.2 in Avanesyan et al. (2020))**.** The functions $\mu : \mathbb{R}^{d_X} \to \mathbb{R}^{d_S}$, $\sigma : \mathbb{R}^{d_X} \to \mathbb{R}^{d_W \times d_S}$ are continuous. The columns of ρ belong to the range of left-multiplication by $\sigma(x)$ for all $x \in \mathbb{R}^{d_X}$.

Assumption F.5 (EVE Condition in Avanesyan et al. (2020))**.** For some $p \in [0,1]$,

$$\rho^\top \rho = pI,$$

where I is the identity matrix. Note that when $p = 1$, ρ is a vector and thus we define $p := \rho^\top \rho$.

F.3.2 Concrete Example

We consider a more concrete example of EVE satisfying the formulation and assumptions in Appendix F.3.1. Specifically, we use D_μ, D_σ, and D_λ to denote diagonal matrices. Let $D(x)$ denote the diagonal matrix whose diagonal is x. We use $x^{\circ k}$ for any $k \in \mathbb{R}$ to denote the component-wise power operation (Hadamard power).

We define

$$\begin{aligned}
\mu(x) &:= D_\mu x^{\circ \frac{3}{2}} \\
\sigma(x) &:= D_\sigma D(x) \\
\kappa(x) &:= \rho^{-1} D_\kappa D(x^{\circ \frac{1}{2}}).
\end{aligned}$$

Then, we have

$$\lambda(x) = D_\sigma^{-1} D_\mu x^{\circ \frac{1}{2}}.$$

Further, we pose

$$\rho^\top \rho = \rho \rho^\top = I.$$

Then,

$$\begin{aligned}
&\lambda(x) = \left(\sigma(x)^{-1}\right)^\top \mu(x) = D_\sigma^{-1} x^{\circ \frac{1}{2}} \text{ and } \lambda(x)^\top \lambda(x) = D_\sigma^{-2} x, \\
&\kappa(x)^\top \kappa(x) = D_\kappa D(x^{\circ \frac{1}{2}}) \left(\rho^{-1}\right)^\top \rho^{-1} D_\kappa D(x^{\circ \frac{1}{2}}) = D_\kappa^2 D(x), \\
&\Gamma \kappa(x)^\top \rho^\top \lambda(x) = \Gamma D(x^{\circ \frac{1}{2}}) D_\kappa \left(\rho^{-1}\right)^\top \rho^\top D_\sigma^{-1} x^{\circ \frac{1}{2}} = \Gamma D(x^{\circ \frac{1}{2}}) D_\kappa D_\sigma^{-1} x^{\circ \frac{1}{2}} = \Gamma D_\kappa D_\sigma^{-1} x.
\end{aligned}$$

Such a setup satisfies Equation (16).

F.3.3 Policy Functional Form

The policy functional form of the EVE model with Markovian stochastic factors can be derived as:

Lemma F.6. *Under the assumptions in Appendices F.3.1 and F.3.2, the optimal policy function follows:*

$$\pi_t^* = \frac{1}{\gamma} \sigma(X_t)^{-1} \left(\lambda(X_t) + q\rho\kappa(X_t) k_2(t)^\top \right),$$

with

$$\begin{aligned}
&\frac{dk_2^i(t)}{dt} + \frac{1}{2} L_i (k_2(t)^i)^2 + \sum_{j=1}^{d_X} (M+N)^{ij} k_2(t)^j + \frac{\Gamma}{2q} \Lambda^i = 0, \quad i = 1, 2, \cdots, d_X \\
&\frac{dk_1(t)}{dt} + \omega^\top k_2(t) = 0.
\end{aligned}$$

For the specific example in Appendix F.3.2, in FaLPO, we parameterize the candidate policy as

$$\pi(t, Y_t, Z_t; \theta_\phi, \theta_\pi) = \Pi(t, Y_t, Z_t; \theta_\phi, \theta_\pi) = \phi(Y_t)^{\frac{1}{2}} k(t; \theta_\pi).$$

F.3.4 Model Calibration

Following the derivations in Appendix E.2, we can derive the calibration objective as:

$$L(\theta_S) := -\min_{\theta_S=(C_1,C_2)} \mathbb{E}\left\|\Delta \log(S_t) - C_1\phi(Y_t;\theta_\phi)^{\circ\frac{3}{2}}\Delta t - C_2\phi(Y_t;\theta_\phi)^{\circ 2}\Delta t\right\|_2^2.$$

G Solutions of Riccati Differential Equations

According to the analysis in Section F, the optimal policy function is closely related to the solutions of Riccati differential equations, which also have closed-form solutions. Specifically, with abuse of notation, let A, B and D be $p \times p$ matrices, and $X(t) : [0, T] \to \mathbb{R}^{p\times p}$ as a function of t solving the following Riccati differential equation:

$$\begin{aligned} \frac{\partial dX(t)}{dt} &= A^\top X(t) + X(t)A - X(t)BB^\top X(t) + D^\top D, \\ X(0) &= X_0. \end{aligned} \tag{18}$$

Following the analysis and assumptions in (Behr et al., 2021), the unique symmetric positive stabilizing solution of $X(t)$ follows:

$$X(t) = X_\infty - e^{t\hat{A}^\top}\big(X_\infty - X_0\big)\big[I - (X_L - e^{t\hat{A}}X_L e^{t\hat{A}^\top})(X_\infty - X_0)\big]^{-1}e^{t\hat{A}},$$

where

$$\hat{A}X_L + X_L\hat{A}^\top + BB^\top = 0,$$

with $\hat{A} := A - BB^\top X_\infty$, and

$$0 = A\top X_\infty + X_\infty A + D^\top D.$$

Note that with Equation (18) we can further derive the policy functional forms without using neural networks to parameterize time-dependent functions.

H Extension to Linear Quadratic Control (LQC)

FaLPO can also be applied to decision-making problems other than portfolio optimization. To implement FaLPO, one needs to first construct a neural stochastic factor model combining factor representation with a continuous-time model. Then, the policy learning is conducted while leveraging policy functional form and model calibration. As an example, we implement FaLPO to linear quadratic control (LQC), and detail modeling (Section H.1), policy functional form (Section H.2) and model calibration (Section H.3).

H.1 Modeling

We consider the problem of LQC (Sun & Yong, 2020) but with stochastic factor X_t following an OU process. With slight abuse of notation, we use S_t to denote the sate variable in this section:

$$\begin{aligned} dS_t &= (BS_t + UA_t + X_t)\,dt + \sum_{j=1}^{d_W} D_j A_t\,dW_t^j, \\ X_t &= \mu X_t\,dt + v\,dW_t, \end{aligned} \tag{19}$$

where B, U, μ, v, and D_j are redefined as matrices with appropriate dimensions. With $A_t = \pi(\cdot)$ following the policy π, we aim to solve

$$\max_\pi V(\pi) \text{ with } V(\pi) := \mathbb{E}_\pi\left[\int_0^T \left[(QS_t)^\top S_t + (RA_t)^\top A_t\right]dt + (GS_T)^\top S_T\right], \tag{20}$$

with Q, R, and G as known matrices with appropriate dimensions, and T is terminal time. Further, we apply the modeling strategy in Section 3.1 and aim to learn the representation of stochastic factors:

$$X_t = \phi(Y_t;\theta_\phi^*).$$

H.2 Policy Functional Form

By taking Ξ_t (the combination of S_t and X_t) as the state variables, we can reformulate the problem as a classic LQC problem:

$$d\Xi_t = B^{\Xi}\Xi_t + U^{\Xi}A_t + \sum_{j=1}^{d_W}(D_j^{\Xi}A_t + \beta_t^{\Xi})dW_t^j,$$

with all the coefficients redefined. Then, under common assumptions in Sun & Yong (2020); Yong & Zhou (1999), it can be derived that the optimal policy satisfies:

$$\tilde{\pi}^*(t,\xi) = \Lambda^{\Xi}(K^{\Xi}(t))^{-1}(U^{\Xi})^{\top}K^{\Xi}(t)\xi,$$

where

$$\Lambda^{\Xi}(K^{\Xi}(t)) = R + \sum_{j=1}^{d_W}(D_j^{\top}K^{\Xi}(t)D_j).$$

Also, $K^{\Xi}(t)$ solves the differential Riccati equation:

$$\begin{aligned} K^{\Xi}(t) = &- e^{(B^{\Xi})^{\top}(T-t)}G^{\Xi}e^{B^{\Xi}(T-t)} \\ &- \int_t^T e^{(B^{\Xi})^{\top}(T-\tau)}K^{\Xi}(\tau)^{\top}U^{\Xi}\big(\Lambda^{\Xi}(K^{\Xi}(\tau))^{\top}\big)^{-1}(U^{\Xi})^{\top}K^{\Xi}(\tau)e^{(B^{\Xi})^{\top}(T-\tau)}d\tau, \end{aligned}$$

with

$$K^{\Xi}(T) = 0.$$

Therefore, we can formulate the candidate policy as

$$\pi(t,S_t,Y_t;\theta_\phi,\theta_\pi) = \Pi(t,S_t,Y_t;\theta_\phi,\theta_\pi) = k_1(t;\theta_\pi)S_t + k_2(t;\theta_\pi)\phi(Y_t;\theta_\phi). \tag{21}$$

H.3 Model Calibration

According to Equation (19) and following the derivation strategy in Appendix E.2, we can derive the negative mean square loss for LQC as

$$L(\theta_\phi,\theta_S) := \mathbb{E}\big[\,\|S_{t+\Delta t}S_t - \phi(Y_t;\theta_\phi)\Delta t - C_1S_t - C_2A_t\|_2^2\,\big], \tag{22}$$

with $\theta_S = \{C_1, C_2\}$.

As a summary, to apply FaLPO to LQC with stochastic factors, we parameterize candidate policies following Equation (21) and maximize

$$(1-\lambda V(\theta_\phi,\theta_\pi)) + \lambda L(\theta_\phi,\theta_S),$$

with V in Equation (20) and L in Equation (22).

I Extended Results for Theorem 4.1

I.1 Assumptions and Definitions

To start with, we consider stochastic factor models such that the optimal feedback admissible policy admits a functional form as

$$\tilde{\pi}_t^* = \Pi(t,X_t;\theta_\pi^*).$$

Also, we consider the L function such that the true data generating parameters $\theta_S^*, \theta_\phi^*$ satisfy

$$\theta_S^*, \theta_\phi^* \in \operatorname*{arg\,max}_{\theta_\phi,\theta_S} L(\theta_\phi,\theta_S), \tag{23}$$

while other options for L can also be empirically used in our method.

Definition I.1. For a continuous-time policy $\tilde{\pi}_t := \Pi(t, S_t, Z_t, \phi(Y_t; \theta_\phi); \theta_{\tilde{\pi}})$, we define its value function as

$$\tilde{V}(\theta_\phi, \theta_\pi) := \mathbb{E}[U(Z_T^{\tilde{\pi}})].$$

Accordingly, we define the continuous-time version objective function as

$$\tilde{H}(\theta_\phi, \theta_{\tilde{\pi}}, \theta_S) := (1-\lambda)\tilde{V}(\theta_\phi, \theta_{\tilde{\pi}}) + \lambda L(\theta_\phi, \theta_S).$$

Definition I.2. For $t \in [m\Delta t, (m+1)\Delta t)$, define $\lfloor t \rfloor := m\Delta t$ and $\lfloor \tilde{\pi}_t^* \rfloor := \tilde{\pi}_{\lfloor t \rfloor}^*$.

Definition I.3. For the continuous-time optimal policy $\tilde{\pi}^*$, we use $\lfloor \tilde{\pi}^* \rfloor$ to denote the piece-wise constant version $\tilde{\pi}^*$. We use $\tilde{Z}_t^{\lfloor \tilde{\pi}^* \rfloor}$ to denote the wealth process when implementing the optimal continuous-time policy $\tilde{\pi}(\cdot; \theta_\phi^*, \theta_\pi^*)$ in the piece-wise constant manner. Specifically,

$$\begin{aligned} d\tilde{Z}_t^{\lfloor \tilde{\pi}^* \rfloor} :=& \tilde{Z}_{\lfloor t \rfloor}^{\lfloor \tilde{\pi}^* \rfloor} \sum_{i=1}^{d_S} \frac{(\tilde{\pi}_{\lfloor t \rfloor}^*)^i dS_t^i}{S_{\lfloor t \rfloor}^i} \\ =& \sum_{i=1}^{d_S} \Bigg\{ \Pi^i(\lfloor t \rfloor, X_{\lfloor t \rfloor}; \theta_{\tilde{\pi}}^*) f_S^i(X_t; \theta_S^*) \frac{S_t^i}{S_{\lfloor t \rfloor}^i} \tilde{Z}_{\lfloor t \rfloor}^{\lfloor \tilde{\pi}^* \rfloor} dt \\ & + \Pi^i(\lfloor t \rfloor, X_{\lfloor t \rfloor}; \theta_{\tilde{\pi}}^*) \sum_{j=1}^{d_W} g_S^{ij}(X_t; \theta_S^*) \frac{S_t^i}{S_{\lfloor t \rfloor}^i} \tilde{Z}_{\lfloor t \rfloor}^{\lfloor \tilde{\pi}^* \rfloor} dW_t^j \Bigg\}. \end{aligned}$$

Further, remember $\tilde{Z}_t^{\tilde{\pi}^*}$ is used to denote the continuous-time wealth process under the policy $\tilde{\pi}^*$. By the dynamics of continuous-time wealth process $\tilde{Z}_t^{\tilde{\pi}}$ in Section 2.3 the dynamics of $\tilde{Z}_t^{\tilde{\pi}^*}$ is derived as

$$\frac{d\tilde{Z}_t^{\tilde{\pi}^*}}{\tilde{Z}_t^{\tilde{\pi}^*}} = \Pi(t, X_t; \theta_{\tilde{\pi}}^*)^\top f_S(X_t; \theta_S^*) dt + \Pi(t, X_t; \theta_{\tilde{\pi}}^*)^\top g_S(X_t; \theta_S^*)^\top dW_t.$$

Assumption I.4. For each $R > 0$, if $\|x\| \le R$ and $t \le T$, we assume that there exists a $C_R > 0$ such that

$$\|\Pi(t, x; \theta_\pi^*)\| \vee \|f_S(x; \theta_S^*)\| \vee \|g_S(x; \theta_S^*)\| \vee \|f_X(x; \theta_S^*)\| \vee \|g_X(x; \theta_S^*)\| \le C_R,$$

and $\Pi(t, x; \theta_\pi^*)$ is locally Lipschitz with Lipschitz constant C_R.

For some $p > 2$, there exists a constant A such that

$$\mathbb{E}\big[\sup_{0 \le t \le T} |\tilde{Z}_t^{\tilde{\pi}^*}|^p\big] \vee \mathbb{E}\big[\sup_{0 \le t \le T} |\tilde{Z}_t^{\lfloor \tilde{\pi}^* \rfloor}|^p\big] \vee \mathbb{E}\big[\sup_{0 \le t \le T} \|X_t\|^p\big] \vee \mathbb{E}\big[\sup_{0 \le t \le T} \|\log(S_t)\|^p\big] \le A.$$

Note that Assumption I.4 requires the stochastic processes to have bounded high-order moments. For a specific model like Kim–Omberg, this is not guaranteed to hold for every initial value and SDE coefficient, but one can derive model-specific sufficient conditions for Assumption I.4. In practice when implementing the method, we calculate the empirical moments of wealth, factors and asset prices to approximately check whether Assumption I.4 holds.

With Assumption I.4, we define a stopping time:

Definition I.5. For $R > 0$, define a stopping time

$$\tau_R := \left\{ \inf_{0 \le t \le T} | \, |\tilde{Z}_t^{\tilde{\pi}^*}| \ge R \text{ or } \|X_t\| \ge R \text{ or } \|\log(S_t)\| \ge R \text{ or } |\tilde{Z}_t^{\lfloor \tilde{\pi}^* \rfloor}| \ge R \right\}.$$

Assumption I.6. The utility function $U(z)$ has a linear bound on $\mathcal{Z}$:

$$|U(z)| \le C_U(|z| + 1).$$

Note that Assumption I.6 holds as long as the utility function is bounded at the smallest value in $\mathcal{Z}$. Specifically for power utility, Assumption I.6 is equivalent to setting $\gamma \in (0, 1)$.

Assumption I.7. There exists $\Delta t' > 0$ such that for any $\Delta t < \Delta t'$, $\lfloor \tilde{\pi}^* \rfloor$ is also an admissible policy.

I.2 Lemmas

Lemma I.8. *Consider n non-negative constants $c_1, c_2, \cdots, c_n$. The following inequality is true:*

$$(\sum_{i=1}^{n} c_i)^2 \leq n \sum_{i=1}^{n} c_i^2.$$

Proof. The proof follows the Cauchy-Schwartz inequality. □

Lemma I.9. *$(\theta_\phi^*, \theta_{\tilde{\pi}}^*, \theta_S^*)$ maximizes both $\tilde{V}(\theta_\phi, \theta_{\tilde{\pi}})$ and $L(\theta_\phi, \theta_S)$.*

Proof. Since $\theta_{\tilde{\pi}^*}$ is defined to be the optimal parameter for the continuous-time policy and θ_ϕ^* is defined to be the true data generating parameter, then $(\theta_\phi^*, \theta_\pi^*)$ maximize $\tilde{V}$. By Equation (23), $(\theta_\phi^*, \theta_S^*)$ maximize L. □

Lemma I.10. *For any $\delta > 0$,*

$$\mathbb{E}[\sup_{0\leq t\leq T}(\tilde{Z}_t^{\lfloor\tilde{\pi}^*\rfloor} - \tilde{Z}_t^{\tilde{\pi}^*})^2] \leq \mathbb{E}\big[\sup_{0\leq t\leq T}(\tilde{Z}_{t\wedge\tau_R}^{\lfloor\tilde{\pi}^*\rfloor} - \tilde{Z}_{t\wedge\tau_R}^{\tilde{\pi}^*})^2\big] + \frac{2^{p+1}\delta A}{p} + \frac{(p-2)8A}{p\delta^{2/(p-2)}R^p}.$$

Proof. Proof by applying Young's inequality. See derivation in Higham et al. (2002, Equation (2.8)). □

Lemma I.11. *For any $t \leq \tau_R$, the difference between the coefficients of the dynamics of $\tilde{Z}_t^{\tilde{\pi}^*}$ and $\tilde{Z}_t^{\lfloor\tilde{\pi}^*\rfloor}$ are bounded by:*

$$\begin{aligned}
&\left|\sum_{i=1}^{d_S}\Pi(t, X_t; \theta_\pi^*) f_S^i(X_t; \theta_S^*)\tilde{Z}_t^{\tilde{\pi}^*} - \sum_{i=1}^{d_S}\Pi(\lfloor t\rfloor, X_{\lfloor t\rfloor}; \theta_\pi^*) f_S^i(X_t; \theta_S^*)\tilde{Z}_{\lfloor t\rfloor}^{\lfloor\tilde{\pi}^*\rfloor}\frac{S_t^i}{S_{\lfloor t\rfloor}^i}\right|^2 \\
&\leq 5d_S^2\exp(2R)C_R^4\big[\exp(2R)R^2|t-\lfloor t\rfloor|^2 + \exp(2R)R^2\left|X_t - X_{\lfloor t\rfloor}\right|^2 \\
&+ R^2\left\|S_{\lfloor t\rfloor} - S_t\right\|^2 + \exp(2R)\left|\tilde{Z}_t^{\tilde{\pi}^*} - \tilde{Z}_t^{\lfloor\tilde{\pi}^*\rfloor}\right|^2 + \exp(2R)\left|\tilde{Z}_t^{\lfloor\tilde{\pi}^*\rfloor} - \tilde{Z}_{\lfloor t\rfloor}^{\lfloor\tilde{\pi}^*\rfloor}\right|^2\big],
\end{aligned}$$

and

$$\begin{aligned}
&\left|\sum_{i=1}^{d_S}\left[\Pi(\lfloor t\rfloor, X_{\lfloor t\rfloor}; \theta_\pi^*)\sum_{j=1}^{d_W}\big(g_S^{ij}(X_t; \theta_S^*)\frac{S_t^i}{S_{\lfloor t\rfloor}^i}\tilde{Z}_{\lfloor t\rfloor}^{\lfloor\tilde{\pi}^*\rfloor}\big)\right] - \sum_{i=1}^{d_S}\left[\Pi(t, X_t; \theta_\pi^*)\sum_{j=1}^{d_W}\big(g_S^{ij}(X_t; \theta_S^*)\tilde{Z}_t^{\tilde{\pi}^*}\big)\right]\right|^2 \\
&\leq 5d_S^2\exp(2R)C_R^4\Bigg[\exp(2R)R^2|t-\lfloor t\rfloor|^2 + \exp(2R)R^2\left|X_t - X_{\lfloor t\rfloor}\right|^2 \\
&+ R^2\left\|S_{\lfloor t\rfloor} - S_t\right\|^2 + \exp(2R)\left|\tilde{Z}_t^{\tilde{\pi}^*} - \tilde{Z}_t^{\lfloor\tilde{\pi}^*\rfloor}\right|^2 + \exp(2R)\left|\tilde{Z}_t^{\lfloor\tilde{\pi}^*\rfloor} - \tilde{Z}_{\lfloor t\rfloor}^{\lfloor\tilde{\pi}^*\rfloor}\right|^2\Bigg].
\end{aligned}$$

Proof. By triangle inequality

$$\begin{aligned}
&\left|\sum_{i=1}^{d_S}\tilde{\pi}_t^i f_S^i(X_t; \theta_S^*)\tilde{Z}_t^{\tilde{\pi}^*} - \sum_{i=1}^{d_S}\tilde{\pi}_{\lfloor t\rfloor}^i f_S^i(X_t; \theta_S^*)\tilde{Z}_{\lfloor t\rfloor}^{\lfloor\tilde{\pi}^*\rfloor}\frac{S_t^i}{S_{\lfloor t\rfloor}^i}\right| \\
\leq &\sum_{i=1}^{d_S}\frac{1}{S_{\lfloor t\rfloor}^i}\left|f_S^i(X_t; \theta_S^*)\right|\Big(\left|\tilde{\pi}_t^i\tilde{Z}_t^{\tilde{\pi}^*}S_{\lfloor t\rfloor}^i - \tilde{\pi}_{\lfloor t\rfloor}^i\tilde{Z}_t^{\tilde{\pi}^*}S_{\lfloor t\rfloor}^i\right| \\
&+ \left|\tilde{\pi}_{\lfloor t\rfloor}^i\tilde{Z}_t^{\tilde{\pi}^*}S_{\lfloor t\rfloor}^i - \tilde{\pi}_{\lfloor t\rfloor}^i\tilde{Z}_{\lfloor t\rfloor}^{\lfloor\tilde{\pi}^*\rfloor}S_{\lfloor t\rfloor}^i\right| + \left|\tilde{\pi}_{\lfloor t\rfloor}^i\tilde{Z}_{\lfloor t\rfloor}^{\lfloor\tilde{\pi}^*\rfloor}S_{\lfloor t\rfloor}^i - \tilde{\pi}_{\lfloor t\rfloor}^i\tilde{Z}_{\lfloor t\rfloor}^{\lfloor\tilde{\pi}^*\rfloor}S_t^i\right|\Big).
\end{aligned}$$

For any $t \leq \tau_R$, we can further bound the right hand side by Assumption I.4

$$\begin{aligned}
&\left|\sum_{i=1}^{d_S}\tilde{\pi}_t^i f_S^i(X_t; \theta_S^*)\tilde{Z}_t^{\tilde{\pi}^*} - \sum_{i=1}^{d_S}\tilde{\pi}_{\lfloor t\rfloor}^i f_S^i(X_t; \theta_S^*)\tilde{Z}_{\lfloor t\rfloor}^{\lfloor\tilde{\pi}^*\rfloor}\frac{S_t^i}{S_{\lfloor t\rfloor}^i}\right| \\
\leq &d_S\exp(R)C_R^2\big[\exp(R)R\big(|t-\lfloor t\rfloor| + \left\|X_t - X_{\lfloor t\rfloor}\right\|\big) \\
&+ \exp(R)\Big(\left|\tilde{Z}_t^{\tilde{\pi}^*} - \tilde{Z}_t^{\lfloor\tilde{\pi}^*\rfloor}\right| + \left|\tilde{Z}_t^{\lfloor\tilde{\pi}^*\rfloor} - \tilde{Z}_{\lfloor t\rfloor}^{\lfloor\tilde{\pi}^*\rfloor}\right|\Big) + R\left\|S_{\lfloor t\rfloor} - S_t\right\|\big].
\end{aligned}$$

Then, by Lemma I.8

$$
\begin{aligned}
&\left|\sum_{i=1}^{d_S}\tilde{\pi}_t^i f_S^i(X_t;\theta_S^*)\tilde{Z}_t^{\tilde{\pi}^*}-\sum_{i=1}^{d_S}\tilde{\pi}_{\lfloor t\rfloor}^i f_S^i(X_t;\theta_S^*)\tilde{Z}_{\lfloor t\rfloor}^{\lfloor\tilde{\pi}^*\rfloor}\frac{S_t^i}{S_{\lfloor t\rfloor}^i}\right|^2\\
\leq& 5d_S^2\exp(2R)C_R^4\big[\exp(2R)R^2\big(|t-\lfloor t\rfloor|^2+\left|X_t-X_{\lfloor t\rfloor}\right|^2\big)\\
&+\exp(2R)\big(\left|\tilde{Z}_t^{\tilde{\pi}^*}-\tilde{Z}_t^{\lfloor\tilde{\pi}^*\rfloor}\right|^2+\left|\tilde{Z}_t^{\lfloor\tilde{\pi}^*\rfloor}-\tilde{Z}_{\lfloor t\rfloor}^{\lfloor\tilde{\pi}^*\rfloor}\right|^2\big)+R^2\left\|S_{\lfloor t\rfloor}-S_t\right\|^2\big]\\
=& 5d_S^2\exp(2R)C_R^4\big[\exp(2R)R^2|t-\lfloor t\rfloor|^2+\exp(2R)R^2\left|X_t-X_{\lfloor t\rfloor}\right|^2\\
&+R^2\left\|S_{\lfloor t\rfloor}-S_t\right\|^2+\exp(2R)\left|\tilde{Z}_t^{\tilde{\pi}^*}-\tilde{Z}_t^{\lfloor\tilde{\pi}^*\rfloor}\right|^2+\exp(2R)\left|\tilde{Z}_t^{\lfloor\tilde{\pi}^*\rfloor}-\tilde{Z}_{\lfloor t\rfloor}^{\lfloor\tilde{\pi}^*\rfloor}\right|^2\big].
\end{aligned}
$$

Similarly

$$
\begin{aligned}
&\left|\sum_{i=1}^{d_S}\left[\tilde{\pi}_{\lfloor t\rfloor}^i\sum_{j=1}^{d_W}\big(g_S^{ij}(X_t;\theta_S^*)\frac{S_t^i}{S_{\lfloor t\rfloor}^i}\tilde{Z}_{\lfloor t\rfloor}^{\lfloor\tilde{\pi}^*\rfloor}\big)\right]-\sum_{i=1}^{d_S}\left[\tilde{\pi}_t^i\sum_{j=1}^{d_W}\big(g_S^{ij}(X_t;\theta_S^*)\tilde{Z}_t^{\tilde{\pi}^*}\big)\right]\right|^2\\
&\leq 5d_S^2\exp(2R)C_R^4\big[\exp(2R)R^2|t-\lfloor t\rfloor|^2+\exp(2R)R^2\left|X_t-X_{\lfloor t\rfloor}\right|^2\\
&+R^2\left\|S_{\lfloor t\rfloor}-S_t\right\|^2+\exp(2R)\left|\tilde{Z}_t^{\tilde{\pi}^*}-\tilde{Z}_t^{\lfloor\tilde{\pi}^*\rfloor}\right|^2+\exp(2R)\left|\tilde{Z}_t^{\lfloor\tilde{\pi}^*\rfloor}-\tilde{Z}_{\lfloor t\rfloor}^{\lfloor\tilde{\pi}^*\rfloor}\right|^2\big].
\end{aligned}
$$

□

Lemma I.12. *With τ_R defined in Definition I.5,*

$$
\begin{aligned}
&\mathbb{E}\left\|X_{t\wedge\tau_R}-X_{\lfloor t\wedge\tau_R\rfloor}\right\|^2\leq 2C_R^2(\Delta t^2+\Delta t),\\
&\mathbb{E}\left\|S_{t\wedge\tau_R}-S_{\lfloor t\wedge\tau_R\rfloor}\right\|^2\leq 2\exp(2R)C_R^2(\Delta t^2+\Delta t),\\
&\mathbb{E}\left\|\tilde{Z}_{\lfloor t\wedge\tau_R\rfloor}^{\lfloor\tilde{\pi}^*\rfloor}-\tilde{Z}_{t\wedge\tau_R}^{\lfloor\tilde{\pi}^*\rfloor}\right\|^2\leq 2R^2\exp(4R)C_R^4(\Delta t^2+\Delta t).
\end{aligned}
$$

Proof. By the dynamics of X_t and Lemma I.8, we can derive

$$
\mathbb{E}\left\|X_{t\wedge\tau_R}-X_{\lfloor t\wedge\tau_R\rfloor}\right\|^2\leq 2\Delta t\mathbb{E}\int_{m_{t\wedge\tau_R}\Delta t}^{t\wedge\tau_R}\left\|f_X(X_s;\theta_S^*)\right\|^2ds+2\mathbb{E}\left\|\int_{m_{t\wedge\tau_R}\Delta t}^{t\wedge\tau_R}g_X(X_s;\theta_S^*)^\top dW_s\right\|^2,
$$

where $m_{t\wedge\tau_R}$ satisfies $m_{t\wedge\tau_R}\Delta t\leq(t\wedge\tau_R)<(m_{t\wedge\tau_R}+1)\Delta t$. Further, we apply Itô's isometry with stopping time (Lemma D.2), and derive

$$
\mathbb{E}\left\|X_{t\wedge\tau_R}-X_{\lfloor t\wedge\tau_R\rfloor}\right\|^2\leq 2\Delta t\mathbb{E}\int_{m_{t\wedge\tau_R}\Delta t}^{t\wedge\tau_R}\left\|f_X(X_s;\theta_S^*)\right\|^2ds+2\mathbb{E}\int_{m_{t\wedge\tau_R}\Delta t}^{t\wedge\tau_R}\left\|g_X(X_s;\theta_S^*)\right\|^2ds.
$$

By Assumption I.4, we derive

$$
\mathbb{E}\left\|X_{t\wedge\tau_R}-X_{\lfloor t\wedge\tau_R\rfloor}\right\|^2\leq 2C_R^2(\Delta t^2+\Delta t).
$$

Similarly

$$
\mathbb{E}\left\|S_{t\wedge\tau_R}-S_{\lfloor t\wedge\tau_R\rfloor}\right\|^2\leq 2\exp(2R)C_R^2(\Delta t^2+\Delta t),
$$

and

$$
\mathbb{E}\left\|\tilde{Z}_{\lfloor t\wedge\tau_R\rfloor}^{\lfloor\tilde{\pi}^*\rfloor}-\tilde{Z}_{t\wedge\tau_R}^{\lfloor\tilde{\pi}^*\rfloor}\right\|^2\leq 2R^2\exp(4R)C_R^4(\Delta t^2+\Delta t).
$$

□

Lemma I.13.

$$\begin{aligned}\mathbb{E}\big[\sup_{0\le t\le\tau}(\tilde{Z}^{\tilde{\pi}^*}_{t\wedge t_k}-\tilde{Z}^{\lfloor\tilde{\pi}^*\rfloor}_{t\wedge t_k})^2\big]\le&10(T+4)Td_S^2C_R^4\exp(4R)R^2\big[\Delta t^2+2C_R^2(\Delta t^2+\Delta t)\\&+2C_R^2(\Delta t^2+\Delta t)+2\exp(4R)C_R^4(\Delta t^2+\Delta t)\big]\\&+10(T+4)d_S^2C_R^4\exp(4R)\int_0^\tau\mathbb{E}\sup_{0\le r\le s}\Big|\tilde{Z}^{\tilde{\pi}^*}_{r\wedge\tau_R}-\tilde{Z}^{\lfloor\tilde{\pi}^*\rfloor}_{r\wedge\tau_R}\Big|^2ds.\end{aligned}$$

Proof. By Cauchy–Schwarz inequality and the dynamics of $\tilde{Z}^{\tilde{\pi}^*}_t$ and $\tilde{Z}^{\lfloor\tilde{\pi}^*\rfloor}_t$, for any $\tau\le T$

$$\begin{aligned}&\mathbb{E}\big[\sup_{0\le t\le\tau}(\tilde{Z}^{\tilde{\pi}^*}_{t\wedge t_k}-\tilde{Z}^{\lfloor\tilde{\pi}^*\rfloor}_{t\wedge t_k})^2\big]\\\le&2T\mathbb{E}\bigg[\sup_{0\le t\le\tau}\int_0^{t\wedge\tau_R}\bigg|\sum_{i=1}^{d_S}\tilde{\pi}^i_sf^i_S(X_s;\theta^*_S)\tilde{Z}^{\tilde{\pi}^*}_s-\sum_{i=1}^{d_S}\tilde{\pi}^i_{\lfloor s\rfloor}f^i_S(X_s;\theta^*_S)\tilde{Z}^{\lfloor\tilde{\pi}^*\rfloor}_{\lfloor s\rfloor}\frac{S^i_s}{S^i_{\lfloor t\rfloor}}\bigg|^2ds\bigg]\\&+2\mathbb{E}\bigg[\sup_{0\le t\le\tau}\bigg|\sum_{j=1}^{d_W}\int_0^{t\wedge\tau_R}\bigg[\sum_{i=1}^{d_S}\tilde{\pi}^i_sg^{ij}(X_s;\theta^*_S)\tilde{Z}^{\tilde{\pi}^*}_s-\tilde{\pi}^i_{\lfloor s\rfloor}g^{ij}(X_{\lfloor s\rfloor};\theta^*_S)S^i_s/S^i_{\lfloor s\rfloor}\bigg]dW^j_s\bigg|^2\bigg].\end{aligned}$$

Then, by Doob's martingale inequality

$$\begin{aligned}&\mathbb{E}\big[\sup_{0\le t\le\tau}(\tilde{Z}^{\tilde{\pi}^*}_{t\wedge t_k}-\tilde{Z}^{\lfloor\tilde{\pi}^*\rfloor}_{t\wedge t_k})^2\big]\\\le&2T\mathbb{E}\bigg[\sup_{0\le t\le\tau}\int_0^{t\wedge\tau_R}\bigg|\sum_{i=1}^{d_S}\tilde{\pi}^i_sf^i_S(X_s;\theta^*_S)\tilde{Z}^{\tilde{\pi}^*}_s-\sum_{i=1}^{d_S}\tilde{\pi}^i_{\lfloor s\rfloor}f^i_S(X_s;\theta^*_S)\tilde{Z}^{\lfloor\tilde{\pi}^*\rfloor}_{\lfloor s\rfloor}\frac{S^i_s}{S^i_{\lfloor t\rfloor}}\bigg|^2ds\bigg]\\&+8T\mathbb{E}\bigg[\bigg(\sum_{j=1}^{d_W}\int_0^{t\wedge\tau_R}\bigg[\sum_{i=1}^{d_S}\tilde{\pi}^i_sg^{ij}(X_s;\theta^*_S)\tilde{Z}^{\tilde{\pi}^*}_s-\tilde{\pi}^i_{\lfloor s\rfloor}g^{ij}(X_{\lfloor s\rfloor};\theta^*_S)S^i_s/S^i_{\lfloor s\rfloor}\bigg]dW^j_s\bigg)^2\bigg].\end{aligned}$$

Next, we apply Lemma I.11,

$$\begin{aligned}&\mathbb{E}\big[\sup_{0\le t\le\tau}(\tilde{Z}^{\tilde{\pi}^*}_{t\wedge t_k}-\tilde{Z}^{\lfloor\tilde{\pi}^*\rfloor}_{t\wedge t_k})^2\big]\\\le&10(T+4)d_S^2C_R^4\exp(2R)\mathbb{E}\bigg[\int_0^{\tau\wedge\tau_R}\big(\exp(2R)R^2|s-\lfloor s\rfloor|^2+\exp(2R)R^2\big|X_s-X_{\lfloor s\rfloor}\big|^2\\&+R^2\left\|S_{\lfloor s\rfloor}-S_s\right\|^2+\exp(2R)\Big|\tilde{Z}^{\tilde{\pi}^*}_s-\tilde{Z}^{\lfloor\tilde{\pi}^*\rfloor}_s\Big|^2+\exp(2R)\Big|\tilde{Z}^{\lfloor\tilde{\pi}^*\rfloor}_s-\tilde{Z}^{\lfloor\tilde{\pi}^*\rfloor}_{\lfloor s\rfloor}\Big|^2\big)ds\bigg].\end{aligned}$$

Therefore, combined with Lemma I.12,

$$\begin{aligned}\mathbb{E}\big[\sup_{0\le t\le\tau}(\tilde{Z}^{\tilde{\pi}^*}_{t\wedge t_k}-\tilde{Z}^{\lfloor\tilde{\pi}^*\rfloor}_{t\wedge t_k})^2\big]\le&10(T+4)Td_S^2C_R^4\exp(4R)R^2\big[\Delta t^2+2C_R^2(\Delta t^2+\Delta t)\\&+2C_R^2(\Delta t^2+\Delta t)+2\exp(4R)C_R^4(\Delta t^2+\Delta t)\big]\\&+10(T+4)d_S^2C_R^4\exp(4R)\int_0^\tau\mathbb{E}\sup_{0\le r\le s}\Big|\tilde{Z}^{\tilde{\pi}^*}_{r\wedge\tau_R}-\tilde{Z}^{\lfloor\tilde{\pi}^*\rfloor}_{r\wedge\tau_R}\Big|^2ds.\end{aligned}$$

□

Lemma I.14. *With the definitions and assumptions in Appendix I.1,*

$$\lim_{\Delta t\to0}\mathbb{E}[(\tilde{Z}^{\lfloor\tilde{\pi}^*\rfloor}_T-\tilde{Z}^{\tilde{\pi}^*}_T)^2]=0.$$

Proof. By Lemma I.13, we apply the Gronwall inequality and obtain

$$\begin{aligned}
&\mathbb{E}\big[\sup_{0\le t\le T}(\tilde{Z}^{\tilde{\pi}^*}_{t\wedge t_k}-\tilde{Z}^{\tilde{\pi}^*}_{t\wedge t_k})^2\big]\\
&\qquad\le 10(T+4)Td_S^2C_R^4\exp(4R)R^2\big[\Delta t^2+2C_R^2(\Delta t^2+\Delta t)\\
&\qquad+2C_R^2(\Delta t^2+\Delta t)+2\exp(4R)C_R^4(\Delta t^2+\Delta t)\big]\exp(10(T+4)d_S^2C_R^4\exp(4R)).
\end{aligned}$$

Then, combined with Lemma I.10, for any $\delta>0$,

$$\begin{aligned}
&\mathbb{E}[\sup_{0\le t\le T}(\tilde{Z}^{\tilde{\pi}^*}_{t}-\tilde{Z}^{\lfloor\tilde{\pi}^*\rfloor}_{t})^2]\\
&\qquad\le 10(T+4)Td_S^2C_R^4\exp(4R)R^2\big[\Delta t^2+2C_R^2(\Delta t^2+\Delta t)\\
&\qquad+2C_R^2(\Delta t^2+\Delta t)+2\exp(4R)C_R^4(\Delta t^2+\Delta t)\big]\exp(10(T+4)d_S^2C_R^4\exp(4R))\\
&\qquad+\frac{2^{p+1}\delta A}{p}+\frac{(p-2)8A}{p\delta^{2/(p-2)}R^p}.
\end{aligned}$$

Therefore, $\mathbb{E}[\sup_{0\le t\le T}(\tilde{Z}^{\tilde{\pi}^*}_{t}-\tilde{Z}^{\lfloor\tilde{\pi}^*\rfloor}_{t})^2]$ converges to 0 as Δt goes to 0. □

I.3 Proof

For ease of presentation, we define

$$\theta:=(\theta_\phi,\theta_\pi,\theta_S),\ \theta^*:=(\theta^*_\phi,\theta^*_{\tilde{\pi}},\theta^*_S)\text{ and }\theta^*_{\Delta t}:=(\theta^*_{\phi,\Delta t},\theta^*_{\pi,\Delta t},\theta^*_{S,\Delta t}).$$

Note that every discrete-time admissible policy is a continuous-time admissible policy. Thus, the continuous-time admissible policy set includes the discrete-time admissible policy set. Therefore,

$$\tilde{V}(\theta^*)\ge V^*_{\Delta t}.$$

In other words, it is enough to bound $\tilde{V}(\theta^*)-V(\theta^*_{\Delta t})$ for the proof. By Lemma I.9, θ^* maximizes $\tilde{V}$ and L simultaneously, leading to

$$\tilde{V}(\theta^*)-V(\theta^*_{\Delta t})\le\frac{\tilde{H}(\theta^*)-H(\theta^*_{\Delta t})}{1-\lambda}.$$

By Assumption I.7, for $\Delta t\le\Delta t'$, θ^* is also an admissible parameter $\theta^*\in\mathcal{A}$, leading to $H(\theta^*)-H(\theta^*_{\Delta t})\le 0$. Further, for any $\delta>0$, by adding and subtracting equal terms,

$$\begin{aligned}
&\tilde{V}(\theta^*)-V(\theta^*_{\Delta t})\\
\le&\frac{1}{1-\lambda}[\tilde{H}(\theta^*)-H(\theta^*)+H(\theta^*)-H(\theta^*_{\Delta t})]\\
\le&\frac{1}{1-\lambda}\big|\tilde{H}(\theta^*)-H(\theta^*)\big|.
\end{aligned}\tag{24}$$

Next, we focus on $\big|\tilde{H}(\theta^*;\delta)-H(\theta^*;\delta)\big|$, which by definition has

$$\big|\tilde{H}(\theta^*;\delta)-H(\theta^*;\delta)\big|=(1-\lambda)\Big|\mathbb{E}[U(\tilde{Z}^{\tilde{\pi}^*}_T;\delta)-U(\tilde{Z}^{\lfloor\tilde{\pi}^*\rfloor}_T;\delta)]\Big|,$$

where $\lambda L(\theta^*)$ in both $\tilde{H}(\theta^*;\delta)$ and $H(\theta^*;\delta)$ omit each other. By Lemma I.14, we have $\lim_{\Delta t\to 0}\tilde{Z}^{\lfloor\tilde{\pi}^*\rfloor}_T\xrightarrow{P}\tilde{Z}^{\tilde{\pi}^*}_T$. Since $U(z;\delta)$ is a continuous function, we implement the continuous mapping theorem and derive

$$\lim_{\Delta t\to 0}U(\tilde{Z}^{\lfloor\tilde{\pi}^*\rfloor}_T;\delta)\xrightarrow{P}U(\tilde{Z}^{\tilde{\pi}^*}_T;\delta).\tag{25}$$

By assumption I.4, $\left\{\tilde{Z}^{\lfloor\tilde{\pi}^*\rfloor}_T\right\}_{\Delta t<\Delta t'}$ with different finite Δt is uniformly integrable. Then, following Assumption I.6, $U(\tilde{Z}^{\lfloor\tilde{\pi}^*\rfloor}_T;\delta)$ is also uniformly integrable since $U(z;\delta)$ has a linear bound. Combined with Equation (25), we derive

$$\lim_{\Delta t\to 0}\mathbb{E}[U(\tilde{Z}^{\lfloor\tilde{\pi}^*\rfloor}_T;\delta)]\to\mathbb{E}[U(\tilde{Z}^{\tilde{\pi}^*}_T;\delta)],$$

which finishes the proof.

J Extended Results of Theorem 4.2

In this section, we study the non-asymptotic guarantees on the performance of FaLPO.

J.1 Another Version of Theorem 4.2

Definition J.1. For two random vectors v and w, we define the trace of the covariance matrix as

$$\begin{aligned}\mathrm{Var}(v) :=& \mathbb{E}[\|v\|_2^2 - \|\mathbb{E}[v]\|_2^2],\\ \mathrm{Cov}(v,w) :=& \mathbb{E}[v^\top w] - \mathbb{E}[v]^\top \mathbb{E}[w].\end{aligned}$$

Further, we use $\mathrm{Var}_\theta(v)$ and $\mathrm{Cov}_\theta(v,w)$ to denote the conditional version of the two given θ:

$$\begin{aligned}\mathrm{Var}_\theta(v) :=& \mathbb{E}[\|v\|_2^2 - \|\mathbb{E}[v|\theta]\|_2^2\,|\theta],\\ \mathrm{Cov}_\theta(v,w) :=& \mathbb{E}[v^\top w|\theta] - \mathbb{E}[v|\theta]^\top \mathbb{E}[w|\theta].\end{aligned}$$

Note that it is challenging to theoretically analyze a non-convex stochastic optimization (5), while there are various ad-hoc procedures providing good empirical performances. To provide theoretical analysis, in this section, we study a projection-based version of FaLPO (Algorithm 2). Specifically, the learning/optimization process is conducted in a bounded parameter space $\mathcal{B}$, under which we assume that the objective function is strongly concave regarding the parameters.

Algorithm 2 Projected FaLPO

Input: Hyperparameter λ, learning rate η, number of iterations N, the strongly concave region $\mathcal{B}$, and batch size B.
Output: θ_ϕ, θ_π, and θ_S
Initialize neural networks with initial parameters $(\theta_\phi, \theta_\pi, \theta_S) \in \mathcal{B}$.
Parameterize the policy function by (3).
for $n \in [N]$ **do**
  Collect B trajectories.
  Estimate the gradients of H following the procedure in Appendix C with the parameter λ.
  Update θ_S and θ_R with learning rate η by gradients.
  Project the achieved update to $\mathcal{B}$.
end for
Return θ_ϕ, θ_π, and θ_S.

For ease of presentation, we define

$$\theta^* := (\theta^*_\phi, \theta^*_{\bar{\pi}}, \theta^*_S),\ \theta^*_{\Delta t} := (\theta^*_{\phi,\Delta t}, \theta^*_{\pi,\Delta t}, \theta^*_{S,\Delta t}) \text{ and } \theta^\dagger := (\theta^\dagger_{\phi,\Delta t}, \theta^\dagger_{\pi,\Delta t}, \theta^\dagger_{S,\Delta t}).$$

Let θ_n be the estimation after the nth iteration, and $\bar{\theta} := \frac{\sum_{n=0}^{N-1}\theta_n}{N}$ the average estimation. It is a common technique to consider the average estimation $\bar{\theta}$ instead of the final estimations θ_N for such analysis. Then, we provide a new version of Theorem 4.2.

Definition J.2. With the gradient estimations discussed in Appendix C, we define

$$\tilde{\nabla} H_k(\theta) := (1-\lambda)\tilde{\nabla} V_k(\theta) + \lambda \tilde{\nabla} L_k(\theta).$$

Theorem J.3. *With assumptions in Section J.2, $\lambda \in [0,1)$, and $\eta < \frac{1}{C_L}$ as the learning rate,*

$$\begin{aligned}
&\mathbb{E}[V^*_{\Delta t} - V(\bar{\theta})] \\
\leq &\frac{\tilde{H}(\theta^*) - H(\theta^*_{\Delta t})}{1-\lambda} + \frac{H(\theta^*_{\Delta t}) - H(\theta^\dagger)}{1-\lambda} + \frac{C_{\mathcal{B}}\log(N)}{2N(1-\lambda)} \\
&+ \frac{1}{2NB(1-\lambda)}\mathbb{E}\Bigg[\sum_{n=0}^{N-1}\frac{1}{n+1}[(1-\lambda)^2\mathrm{Var}_{\theta_n}\left(\tilde{\nabla}V_k(\theta_n)\right) + \lambda^2\mathrm{Var}_{\theta_n}\left(\tilde{\nabla}L_k(\theta_n)\right) \\
&+ 2\lambda(1-\lambda)\mathrm{Cov}_{\theta_n}(\tilde{\nabla}V_k(\theta_n), \tilde{\nabla}L_k(\theta_n))]\Bigg].
\end{aligned}$$

Also, there exits situations where a $\lambda \in (0,1)$ provides smaller value for $(1-\lambda)^2\mathrm{Var}\left(\tilde{\nabla}H_k(\theta_n)\right) + \lambda^2\mathrm{Var}\left(\tilde{\nabla}L_k(\theta_n)\right) + 2\lambda(1-\lambda)\mathrm{Cov}(\tilde{\nabla}H_k(\theta_n), \tilde{\nabla}R_k(\theta_n))$ than $\lambda = 0$. In other words, there exist cases where tuning λ may provide better performances.

J.2 Assumptions

Assumption J.4. There exits a constant $C_{\mathcal{B}} > 0$ such that the parameter region $\mathcal{B}$ is a convex set and satisfies the following conditions

1. In $\mathcal{B} \subseteq \mathcal{A}$, $H(\theta_{\phi,\Delta t}, \theta_{\pi,\Delta t}, \theta_{S,\Delta t})$ is locally m-strongly concave with a local maximal point $(\theta^\dagger_{\phi,\Delta t}, \theta^\dagger_{P,\Delta t}, \theta^\dagger_{S,\Delta t}) \in \mathcal{B}$.
2. For any $\theta \in \mathcal{B}$, $\|\theta\| \leq C_{\mathcal{B}}$.
3. For any $\theta \in \mathcal{B}$, the expectation of the gradient estimation is bounded by

$$\left\|\mathbb{E}\left[\frac{\sum_{k=1}^B \tilde{\nabla}H_k(\theta)}{B}\right]\right\|^2 \leq C_{\mathcal{B}}.$$

These assumptions are widely used in existing analysis (Papini et al., 2018; Karimi et al., 2019; Agarwal et al., 2021; Bhandari & Russo, 2024; Wang et al., 2020; Xu et al., 2020).

However, even with Algorithm 2, it remains difficult to guarantee that training is confined to region $\mathcal{B}$, which is typically unknown a priori. In practice, a more effective approach is to use widely adopted weight initialization schemes—such as those proposed in (Glorot & Bengio, 2010).

Assumption J.5. At the nth iteration, we use the learning rate as $\eta_{n+1} = \frac{1}{nm}$.

Note that in practice we will tune the learning rate η as a hyperparameter, since we may not know m. However, it is a common practice to set the learning rate as in Assumption J.5 (Hazan & Kale, 2011; Nemirovski et al., 2009; Shalev-Shwartz et al., 2011)

J.3 Technical Lemmas for Theorem 4.2

Lemma J.6. *With Assumption J.4 and J.5, we have*

$$\begin{aligned}
H(\theta^\dagger) - H(\bar{\theta}) \leq &\frac{1}{2N}\sum_{n=0}^{N-1}\left[\frac{1}{n+1}\left\|\frac{\sum_{k=1}^B \tilde{\nabla}H_k(\theta_n)}{B}\right\|^2\right] \\
&+ \frac{1}{N}\sum_{n=0}^{N-1}\left[\left(\nabla H(\theta_n) - \frac{\sum_{k=1}^B \tilde{\nabla}H_k(\theta_n)}{B}\right)^\top(\theta^\dagger - \theta_n)\right].
\end{aligned}$$

Proof. By the strong concavity of H in Assumption J.4,

$$\nabla H(\theta_n)(\theta^\dagger - \theta_n) \geq H(\theta^\dagger) - H(\theta_n) + \frac{m}{2}\left\|\theta_n - \theta^\dagger\right\|^2. \tag{26}$$

Further, since θ_{n+1} is the projection of $\theta_n + \eta_{n+1}\frac{\sum_{k=1}^B \tilde{\nabla} H_k(\theta_n)}{B}$ to $\mathcal{B}$, the projection satisfies

$$\left\|\theta_n + \eta_{n+1}\frac{\sum_{k=1}^B \tilde{\nabla} H_k(\theta_n)}{B} - \theta^\dagger\right\|^2 \geq \left\|\theta_{n+1} - \theta^\dagger\right\|^2,$$

which suggests

$$\begin{aligned}
&\left\|\theta_n - \theta^\dagger\right\|^2 - \left\|\theta_{n+1} - \theta^\dagger\right\|^2 \\
&\geq \left\|\theta_n - \theta^\dagger\right\|^2 - \left\|\theta_n + \eta_{n+1}\frac{\sum_{k=1}^B \tilde{\nabla} H_k(\theta_n)}{B} - \theta^\dagger\right\|^2 \\
&= -\eta_{n+1}\frac{\sum_{k=1}^B \tilde{\nabla} H_k(\theta_n)}{B}^\top \left(2\theta_n + \eta_{n+1}\frac{\sum_{k=1}^B \tilde{\nabla} H_k(\theta_n)}{B} - 2\theta^\dagger\right) \\
&= -\eta_{n+1}^2\left\|\frac{\sum_{k=1}^B \tilde{\nabla} H_k(\theta_n)}{B}\right\|_2^2 - 2\eta_{n+1}\left(\theta_n - \theta^\dagger\right)^\top \frac{\sum_{k=1}^B \tilde{\nabla} H_k(\theta_n)}{B}.
\end{aligned} \tag{27}$$

We reorder Equation (27) and derive

$$\begin{aligned}
-\left(\theta_n - \theta^\dagger\right)^\top \frac{\sum_{k=1}^B \tilde{\nabla} H_k(\theta_n)}{B} \leq &\frac{1}{2\eta_{n+1}}\Bigg(\left\|\theta_n - \theta^\dagger\right\|^2 \\
&+ \eta_{n+1}^2\left\|\frac{\sum_{k=1}^B \tilde{\nabla} H_k(\theta_n)}{B}\right\|_2^2 - \left\|\theta_{n+1} - \theta^\dagger\right\|^2\Bigg).
\end{aligned}$$

Taking the result back to Equation (26):

$$\begin{aligned}
H(\theta^\dagger) - H(\theta_n) \leq &\left(\nabla H(\theta_n) - \frac{\sum_{k=1}^B \tilde{\nabla} H_k(\theta_n)}{B}\right)^\top (\theta^\dagger - \theta_n) \\
&+ \frac{1}{2\eta_{n+1}}\left(\left\|\theta_n - \theta^\dagger\right\|^2 - \left\|\theta_{n+1} - \theta^\dagger\right\|^2 + \eta_{n+1}^2\left\|\frac{\sum_{k=1}^B \tilde{\nabla} H_k(\theta_n)}{B}\right\|^2\right) \\
&- \frac{m}{2}\left\|\theta_n - \theta^\dagger\right\|^2, \\
= &\left(\nabla H(\theta_n) - \frac{\sum_{k=1}^B \tilde{\nabla} H_k(\theta_n)}{B}\right)^\top (\theta^\dagger - \theta_n) + \frac{1}{2}(\eta_{n+1}^{-1} - m)\left\|\theta_n - \theta^\dagger\right\|^2 \\
&- \frac{1}{2\eta_{n+1}}\left\|\theta_{n+1} - \theta^\dagger\right\|^2 + \frac{1}{2}\eta_{n+1}\left\|\frac{\sum_{k=1}^B \tilde{\nabla} H_k(\theta_n)}{B}\right\|^2.
\end{aligned} \tag{28}$$

By averaging over n with Assumption J.5 we get

$$\begin{aligned}
H(\theta^\dagger) - H(\bar{\theta}) \leq & \sum_{n=0}^{N-1} (H(\theta^\dagger) - H(\theta_n))/N \\
\leq & \frac{1}{2N} \sum_{n=0}^{N-1} \left[\frac{1}{n+1} \left\| \frac{\sum_{k=1}^{B} \tilde{\nabla} H_k(\theta_n)}{B} \right\|^2 \right] \\
& + \frac{1}{N} \sum_{n=0}^{N-1} \left[\left(\nabla H(\theta_n) - \frac{\sum_{k=1}^{B} \tilde{\nabla} H_k(\theta_n)}{B} \right)^\top (\theta^\dagger - \theta_n) \right],
\end{aligned}$$

where the first inequality is due to condition 1 of Assumption J.4. □

J.4 Proof of Theorem 4.2

Recall that every discrete-time admissible policy is a continuous-time admissible policy. Thus, the continuous-time admissible policy set includes the discrete-time admissible policy set. Therefore,

$$\tilde{V}(\theta^*) \geq V^*_{\Delta t}.$$

Therefore, it is enough to bound $\tilde{V}(\theta^*) - V(\bar{\theta})$ for the proof. By Lemma I.9, θ^* maximizes $\tilde{V}$ and L simultaneously. Therefore,

$$\tilde{V}(\theta^*) - V(\bar{\theta}) \leq \frac{\tilde{H}(\theta^*) - H(\bar{\theta})}{1-\lambda} = \frac{\tilde{H}(\theta^*) - H(\theta^*_{\Delta t}) + H(\theta^*_{\Delta t}) - H(\theta^\dagger) + H(\theta^\dagger) - H(\bar{\theta})}{1-\lambda}. \tag{29}$$

Then, we use the convergence result for Algorithm 2 detailed by Lemma J.6 :

$$\begin{aligned}
H(\theta^\dagger) - H(\bar{\theta}) \leq & \frac{1}{2N} \sum_{n=0}^{N-1} \left[\frac{1}{n+1} \left\| \frac{\sum_{k=1}^{B} \tilde{\nabla} H_k(\theta_n)}{B} \right\|^2 \right] \\
& + \frac{1}{N} \sum_{n=0}^{N-1} \left[\left(\nabla H(\theta_n) - \frac{\sum_{k=1}^{B} \tilde{\nabla} H_k(\theta_n)}{B} \right)^\top (\theta^\dagger - \theta_n) \right].
\end{aligned} \tag{30}$$

Then, we take expectation on both sides

$$\begin{aligned}
\mathbb{E}[H(\theta^\dagger) - H(\bar{\theta})] \leq & \frac{1}{2N} \sum_{n=0}^{N-1} \mathbb{E} \left[\frac{1}{n+1} \left\| \frac{\sum_{k=1}^{B} \tilde{\nabla} H_k(\theta_n)}{B} \right\|^2 \right] \\
& + \frac{1}{N} \sum_{n=0}^{N-1} \mathbb{E} \left[\left(\nabla H(\theta_n) - \frac{\sum_{k=1}^{B} \tilde{\nabla} H_k(\theta_n)}{B} \right)^\top (\theta^\dagger - \theta_n) \right].
\end{aligned} \tag{31}$$

For the last component of Equation (31), since $\tilde{\nabla} H_k(\theta_n)$ is an unbiased gradient estimator:

$$\begin{aligned}
& \mathbb{E} \left[\left(\nabla H(\theta_n) - \frac{\sum_{k=1}^{B} \tilde{\nabla} H_k(\theta_n)}{B} \right)^\top (\theta^\dagger - \theta_n) \right] \\
& = \mathbb{E} \left[\mathbb{E} \left[\left(\nabla H(\theta_n) - \frac{\sum_{k=1}^{B} \tilde{\nabla} H_k(\theta_n)}{B} \right)^\top (\theta^\dagger - \theta_n) \middle| \theta_n \right] \right] = 0.
\end{aligned}$$

Then, for the first component in Equation (31)

$$
\begin{aligned}
&\mathbb{E}\left[\frac{1}{n+1}\left\|\frac{\sum_{k=1}^{B}\tilde{\nabla}H_k(\theta_n)}{B}\right\|^2\right] \\
=&\mathbb{E}\left[\mathbb{E}\left[\frac{1}{n+1}\left\|\frac{\sum_{k=1}^{B}\tilde{\nabla}H_k(\theta_n)}{B}\right\|^2|\theta_n\right]\right] \\
=&\frac{1}{n+1}\mathbb{E}\left[\mathrm{Var}_{\theta_n}(\frac{\sum_{k=1}^{B}\tilde{\nabla}H_k(\theta_n)}{B})+\left\|\mathbb{E}\left[\frac{\sum_{k=1}^{B}\tilde{\nabla}H_k(\theta_n)}{B}|\theta_n\right]\right\|^2\right] \\
\leq&\frac{1}{n+1}\mathbb{E}\left[\mathrm{Var}_{\theta_n}(\frac{\sum_{k=1}^{B}\tilde{\nabla}H_k(\theta_n)}{B})+C_{\mathcal{B}}^2\right],
\end{aligned}
$$

where the last inequality is due to condition 3 of Assumption J.4. Equation (31) can be further derived as

$$
\mathbb{E}[H(\theta^\dagger)-H(\bar{\theta})]\leq\frac{1}{2N}\sum_{n=0}^{N-1}\mathbb{E}\left[\frac{1}{n+1}\mathrm{Var}_{\theta_n}(\frac{\sum_{k=1}^{B}\tilde{\nabla}H_k(\theta_n)}{B})+\frac{1}{n+1}C_{\mathcal{B}}\right].
$$

As a result,

$$
\begin{aligned}
&\mathbb{E}[H(\theta^*_{\Delta t})-H(\bar{\theta})] \\
=&\mathbb{E}[H(\theta^*_{\Delta t})-H(\theta^\dagger)+H(\theta^\dagger)-H(\bar{\theta})] \\
\leq&H(\theta^*_{\Delta t})-H(\theta^\dagger)+\frac{C_{\mathcal{B}}\log(N)}{2N} \\
&+\mathbb{E}\sum_{n=0}^{N-1}\frac{\eta[(1-\lambda)^2\mathrm{Var}_{\theta_n}\left(\tilde{\nabla}V_k(\theta_n)\right)+\lambda^2\mathrm{Var}_{\theta_n}\left(\tilde{\nabla}L_k(\theta_n)\right)]}{BN(n+1)} \\
&+\mathbb{E}\sum_{n=0}^{N-1}\frac{\eta[2\lambda(1-\lambda)\mathrm{Cov}_{\theta_n}(\tilde{\nabla}V_k(\theta_n),\tilde{\nabla}L_k(\theta_n))]}{BN(n+1)}\Bigg\}.
\end{aligned}
$$

Taking the results back to Equation (29) we finish the proof.

K Extended Results for Synthetic Experiments

For synthetic portfolio optimization, we provide details for drift and volatility (Appendix K.1), data generation (Appendix K.2), hyperparameter tuning (Appendix K.3), and extended experimental results (Appendix K.4). We consider 21-day trading, and generate 1000 trajectories with 21 observations for training, 1000 for validation, and 1000 for testing. We use average terminal utility as a metric to compare different methods.

K.1 Drift and Volatility

Drift and volatility are two important concepts characterising the strength of signal and noise in financial markets. To demonstrate this, for an asset price S_t^i and time interval Δt, define return as:

$$
return_t^i=\frac{S_{t+\Delta t}^i-S_t^i}{S_t^i}.
$$

The $return_t^i$ can be daily, monthly or yearly, depending on the length of Δt. For a specific asset, drift ($f^i(X_t;\theta_S^*)$ in Equation (2)) is approximately the expectation of the return, while volatility ($g^i(X_t;\theta_S^*)$) is approximately the return's standard deviation. Given multiple assets, drift ($f(X_t;\theta_S^*)$) is a vector and volatility ($g(X_t;\theta_S^*)$) is a matrix. When generating synthetic data (Appendix K.2), we fix the scale of drift and vary the scale of volatility, which is defined as the average value of each component.

K.2 Data Generation

We simulate data for S_t and X_t following SDE (6). To this end, drift and volatility are randomly picked while mimicking the historical stock price data, with an average annual return of 0.1 and average annual volatility in $\{0.1, 0.2, 0.3\}$, leading to a daily return around $\frac{0.1}{252}$ and a daily volatility around $\{0.1/252, 0.2/252, 0.3/252\}$. The true representation function is selected as a component-wise exponential operation. Then, we discritize the SDE following the explicit Euler method, and generate data accordingly (Beskos & Roberts, 2005).

The specific configurations for data generation is:

- Define two scalars: C_d, and C_v determining the scale of drift and volatility:

$$C_d = 0.1/252, \text{, and } C_v \in \{0.1/252, 0.2/252, 0.3/252\}.$$

- σ is selected as a random matrix, whose components follow a uniform distribution in $[0.5C_v, 1.5C_v]$.
- v is selected as a random matrix, whose components follow a uniform distribution in $[-1.5C_dC_v, 1.5C_dC_v]$.
- μ is selected as a diagonal matrix whose diagonal components follow a uniform distribution in $[0.9, 1]$.
- The initial values of X are randomly generated from a uniform distribution on $[-2C_d, 2C_d]$.
- The initial prices of assets are randomly generated from a uniform distribution in $[20, 30]$.

Note that the design makes sure that the simulated price has approximately a yearly return of 0.1 and yearly volatility in $\{0.1, 0.2, 0.3\}$. Table 4 reports the experimental setup parameters.

Experiment Configurations	Values
Time Interval Δt	1 (Day)
Terminal Time T	21
Scale of Annual Drift	0.1
Scale of Annual Volatility	$\{0.1, 0.2, 0.3\}$
Number of Simulated Trajectories	1000
Utility Function	$\{Power, Exponential\}$
Risk Aversion γ	$\{0.1, 3, 5, 10\}$
Number of Replications under Each Hyperparameter	5
Compute Resources	AWS ec2 m5ad.24xlarge

Table 4: Setup for synthetic experiments

K.3 Early Stopping and Hyperparameter Tuning

For better performance, we conduct early stopping for all methods using the average validation utility, with the patience as 5 steps (if the performance does not improve for 5 epochs, the training stops.). The considered hyperparameters include the learning rate, λ, and batch size. For each configuration, we conduct training for 5 times, and average the results. We pick the configuration that provided the best average validation utility, and test it on the test data and calculate the average test utility per trajectory. The tuning process is conducted using the software wandb (Biewald, 2020). Table 5 reports the hyperparameter values.

Hyperparameters	Values
patiBatch Size	$\{100, 50\}$
λ	$\{0, 05, 0.1, 0.9\}$
Learning Rate	$\{0.0005, 0.001, 0.01, 0.1\}$

Table 5: Hyperparameters for synthetic experiments

K.4 Synthetic Experiment Results

To gain a more holistic understanding of the performance of FaLPO in a variety of settings, we conduct experiments with different number of stocks to be traded (Appendix K.4.1), different risk preferences (Appendix K.4.2), and alternative utility functions (Appendix K.4.3). Finally, we also compare the performance of various methods under the Merton model as a sanity check (Appendix K.4.4).

K.4.1 Synthetic Experiment Results with Different Dimensions

Tables 6 and 7 report the synthetic experiment results with the number of simulated stocks (d_S) varying in $\{10, 15\}$. FaLPO outperforms the competing methods in all scenarios. Note that the performance is not strictly negatively correlated with the number of dimensions of the problem or the annual volatility in simulation. The reason is that the noise in the problem is indeed determined by the whole volatility matrix σ, which is randomly generated in the synthetic experiment (Appendix K.2). In other words, the dimension and average scale cannot fully characterize the extent of the noise in a synthetic task.

	Annual Volatility in Simulation	0.1	0.2	0.3
Methods	**FaLPO**	$\mathbf{-0.465} \pm 0.446$	$\mathbf{-1.35} \pm 0.155$	$\mathbf{-2.737} \pm 0.219$
	DDPG	-1.650 ± 0.456	-3.30 ± 1.294	-5.495 ± 1.269
	SLAC	-0.750 ± 0.210	-5.50 ± 0.011	-6.160 ± 0.012
	RichID	-3.350 ± 0.111	-5.65 ± 0.102	-6.325 ± 0.048
	CT-MB-RL	-2.850 ± 0.014	-5.35 ± 0.020	-6.160 ± 0.026
	MMMC	-4.723 ± 7.619	-5.602 ± 4.299	-6.124 ± 3.217

Table 6: Average terminal utility after tuning with standard deviation for synthetic data with $d_S = 10$ and $d_W = 10$.

	Annual Volatility in Simulation	0.1	0.2	0.3
Methods	**FaLPO**	$\mathbf{-2.463} \pm 3.744$	$\mathbf{-1.021} \pm 0.278$	$\mathbf{-2.243} \pm 0.547$
	DDPG	-3.976 ± 1.428	-1.443 ± 0.751	-5.205 ± 1.858
	SLAC	-4.749 ± 0.139	-6.129 ± 0.016	-6.526 ± 0.012
	RichID	-4.973 ± 0.448	-6.321 ± 0.038	-6.641 ± 0.022
	CT-MB-RL	-3.074 ± 0.014	-5.714 ± 0.023	-6.363 ± 0.021
	MMMC	-5.388 ± 5.688	-6.465 ± 4.978	-7.155 ± 5.965

Table 7: Average terminal utility after tuning with standard deviation for synthetic data with $d_S = 15$ and $d_W = 15$.

K.4.2 Synthetic Experiment Results with Different values of γ

Tables 8 and 9 report experimental results with $d_S = 10$, $d_W = 10$, and $\gamma \in \{3, 10\}$ for an exponential utility. FaLPO outperforms the competing methods in most scenarios.

	Annual Volatility in Simulation	0.1	0.2	0.3
Methods	**FaLPO**	-0.003 ± 0.0021	$\mathbf{-0.0055} \pm 0.0008$	$\mathbf{-0.0132} \pm 0.0028$
	DDPG	-0.003 ± 0.001	-0.0105 ± 0.006	-0.0205 ± 0.0034
	SLAC	$\mathbf{-0.003} \pm 0.0007$	-0.0153 ± 0.0013	-0.0192 ± 0.0011
	RichID	-0.012 ± 0.0005	-0.0188 ± 0.0002	-0.0211 ± 0.0
	CT-MB-RL	-0.01 ± 0.0	-0.0179 ± 0.0	-0.0206 ± 0.0
	MMMC	-0.0162 ± 0.0212	-0.0194 ± 0.0135	-0.0210 ± 0.0102

Table 8: Average terminal utility after tuning with standard deviation for synthetic data with $\gamma = 10$.

	Annual Volatility in Simulation	0.1	0.2	0.3
Methods	**FaLPO**	$\mathbf{-4.575} \pm 3.325$	$\mathbf{-17.9358} \pm 2.3349$	-56.0405 ± 13.0502
	DDPG	-23.113 ± 4.3472	-51.6559 ± 11.7981	$\mathbf{-50.0399 \pm 13.8451}$
	SLAC	-23.514 ± 11.7077	-68.6816 ± 0.0254	-76.1371 ± 0.0355
	RichID	-44.629 ± 1.8797	-69.481 ± 0.9413	-77.232 ± 0.1091
	CT-MB-RL	-34.842 ± 0.4686	-65.41 ± 0.1331	-75.4364 ± 0.122
	MMMC	-59.2338 ± 77.4511	-70.8667 ± 49.2500	-76.8619 ± 37.448

Table 9: Average terminal utility after tuning with standard deviation for synthetic data with $\gamma = 3$.

K.4.3 Synthetic Experiment Results with Power Utility

We also conduct synthetic experiments maximizing the expected power utility for portfolio optimization. The results are summarized in Figure 5. FaLPO outperforms the competing methods in all scenarios.

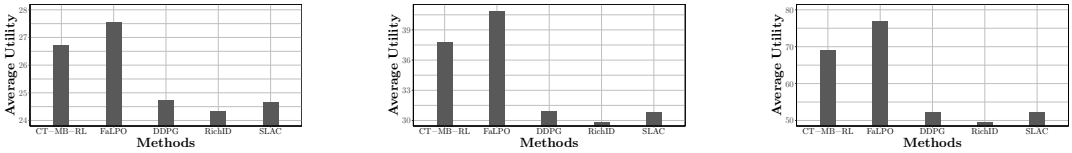

(a) $\gamma = 0.1$ (b) $\gamma = 0.2$ (c) $\gamma = 0.3$

Figure 5: Average Terminal Power Utility

K.4.4 Synthetic Experiment for the Merton Case

As a sanity check, we study a Merton problem where the optimal performance can be mathematically derived, in order to compare the performance of FaLPO to the optimal one. We simulate data following a Merton model in Appendix F.1, with $d_S = 10$, $d_W = 10$. With an exponential utility function with $\gamma = 5$, according to Lemma F.1, the optimal policy can be derived as

$$\tilde{\pi}^* = \frac{\mu(\sigma\sigma^\top)^{-1}}{Z_t}. \tag{32}$$

Further, by taking Equation (32) back into Equation (14), we derive the optimal expected terminal utility

$$\max_{\tilde{\pi}_t} \mathbb{E}_{\tilde{\pi}}[U(Z_T^{\tilde{\pi}})|z_0] = -\frac{e^{-\gamma z_0}}{\gamma} e^{-\frac{1}{2}\mu^\top(\sigma\sigma^\top)^{-1}\mu T},$$

which is the theoretically optimal performance. Then, to implement FaLPO, we generate fake factors which are independent from the asset prices: the optimal policy is not dependent on these factors. Ideally, FaLPO should be able to automatically ignore the fake factors, and deliver performance similar to the theoretically optimal derivation. The results of FaLPO, MMMC, and the theoretically optimal derivation are reported in

Figure 6. Note that FaLPO achieves slightly worse performance compared to the other two. The reason for the slight suboptimality of FaLPO in the Merton case is twofold: i) the expected terminal utility is derived for a continuous-time policy while FaLPO learns a discrete-time policy with time interval Δt; ii) FaLPO uses an over-complicated model with stochastic factors, while the true data generating process follows a Merton model without stochastic factors.

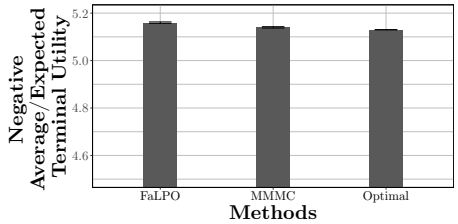

Figure 6: Negative average terminal utility of FaLPO, MMMC, and negative expected optimal terminal utility. The smaller the better.

L Extended Results of Real-World Stock Trading

L.1 Protocol

We consider 21-day stock trading in four different stock sectors using the daily stock price data from Yahoo finance between January 4, 2006 and April 1, 2022. More specifically, we use the adjusted close price as the daily trading price. For factors, we consider economic indexes, technical analysis indexes (generated by python package TA), and sector-specific factors such as oil prices, gold prices, and related ETF prices, leading to around 30 factors for each sector. In each sector we select 10 stocks according to the availability and trading volume in the considered time range. The considered sectors, stocks, and the factors are provided in Table 10. We consider the same competing methods in Section 5.1 and compare the performance using the average achieved terminal utility over different trajectories as the metric. The larger the utility the better.

Sectors	Stocks	Factors
Energy	APA, COP, CVX, HAL, HES, MRO, OKE, OXY, VLO, WMB	SP500 returns, MACD of stock prices, RSI of stock prices, oil prices, gasoline prices US Dollar/USDX - Index - Cash (DX-Y.NYB)
Industrial	BA, CAT, DE, EMR, ETN, GE, HON, LMT, LUV, PNR,	SP500 returns, MACD of stock prices, RSI of stock prices, ETF prices including DIA, EXI, IYJ and VIS
Materials	APD, AVY, BLL, DD, ECL, FMC, IFF, IP, NEM, VMC	SP500 returns, MACD of stock prices, RSI of stock prices, gold prices, silver prices, ETF prices including IYM and VAW

Table 10: Selected stocks and factors

L.2 Extra Penalties

For real-world experiments, we consider two extra penalty terms for better stability. The first penalty is the model calibration loss discussed in Appendix E.3. Given a trajectory with time interval Δt, $\tau := \{t_i, s_{t_i}, x_{t_i} \mid i \in [m]\}$, it is defined as

$$-\lambda_1 \min_{C,b} \sum_{i=1}^{m} \left\| \phi(X_{t_{i+1}}) - C\phi(X_{t_i}) - b \right\|_2^2,$$

where C is a matrix and b a vector of proper dimensions. As discussed in Appendix E.3, this penalty encourages a simple representation function ϕ. The second penalty is the negative sample variance of the

terminal wealth, with the parameter λ_2 determining its strength. The intuition of this penalty is to further penalize the instability of the algorithm performance. The second penalty is implemented for all the competing methods except MMMC for a fair comparison.

L.3 Train-Validation-Test Split by Sliding Window

We detail the sliding window method for train-validation-test split for real-world portfolio optimization experiments (Figure 7). In financial markets, the dynamics under asset prices and factors vary over time, leading us to construct a sliding window on the dataset for training, validation and testing. Specifically, given a dataset of asset prices and observed factors, we construct several windows of observations of equal length. We divide each window into three contiguous periods, the first used for training, the second for validation, and the third for testing. We refer to the length (in days) of the training period as the training size (same for validation and test periods).

After constructing one window, we move the start time point by a fixed number of days (the window gap), and construct the second window. A given method is trained on the training set of each window separately, and then validated and tested on the corresponding validation and test sets. The final validation and test performances are calculated by averaging over each window. The experimental setup is summarized in Table 11. We report the considered hyperparameter values in Table 12.

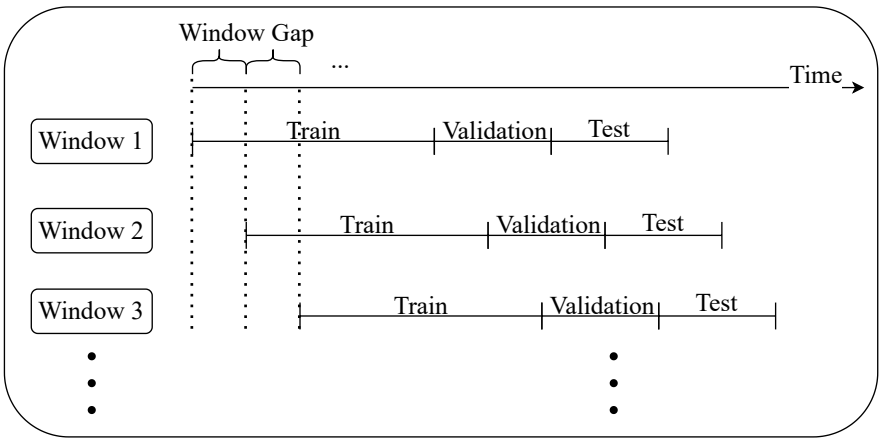

Figure 7: Demonstration of sliding window.

Experiment Configurations	Values
Time Interval Δt	1 (Day)
Terminal Time T	21
Utility Function	*Exponential*
Risk Aversion γ	5
Number of Replications under Each Hyperparameter	10
Compute Resources	AWS ec2 m5ad.24xlarge

Table 11: Setup for real-world experiments.

Hyperparameters	Values
Batch Size	$\{100, 200, 400\}$
λ	$\{0.1, 0.5, 0.9\}$
Learning Rate	$\{0.0005, 0.001, 0.01, 0.1\}$
Window Gap	$\{63, 126\}$
Train Size	$\{1260\}$
Validation Size	$\{63\}$
Test Size	$\{63\}$

Table 12: Hyperparameters for real-world experiments

L.4 Sensitivity Analysis on λ

According to Equation (5), the value of λ determines the weight of the FaLPO model calibration. In this section, we conduct sensitivity analysis of FaLPO on λ. Under the same protocol as the experiments in Section 5.2, we also report FaLPO with different values of λ when applied to different sectors. The results are reported in Figure 8. Compared to the case without model calibration ($\lambda = 0$), a small non-zero λ provides higher terminal utilities and lower variance. This observation justifies our method of incorporating model calibration into policy learning. Then, when λ gets bigger and close to one, the performance of FaLPO decays while the variance also gets smaller.

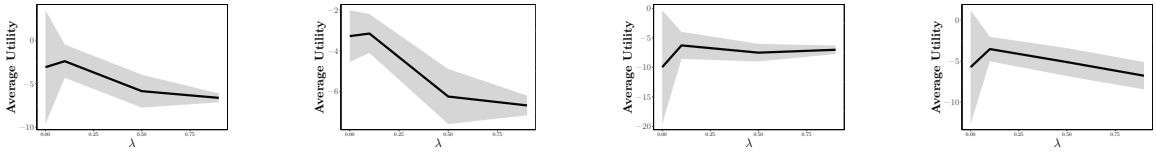

(a) Oil (b) Material (c) Industrials (d) Mix

Figure 8: Sensitivity analysis for λ

L.5 More Information on Competing Methods

Here we provide more information for the implemented competing methods. We focus on policy learning methods, without studying other performance improving techniques like data augmentation or feature engineering which can be easily applied to FaLPO. Further, for a thorough comparison, we select four diverse methods that summarize the existing policy-learning methods for portfolio optimization. For a fair comparison, all methods take asset price data and factors as input.

- DDPG is implemented with the gradient estimation detailed in Appendix C and also discussed in Nan et al. (2022); Xiong et al. (2018); Jiang et al. (2017). This design makes sure that DDPG can leverage offline data without exploration.
- SLAC (Lee et al., 2020) learns a representation of factors jointly with policy learning. But in this process, no parametric models are used.
- RichID (Mhammedi et al., 2020) falls into the category of model-based policy learning like Yu et al. (2019). It first learns the representation of factors and then conducts policy learning. In this process, both steps take advantage of a parametric model. For better performance in portfolio optimization, we pick Kim-Omberg as the used model, instead of LQR as RichID originally proposed.
- CT-MB-RL is a policy gradient method optimizing the performance objective using the policy functional form derived from continuous-time models, but without factor representation learning.

We also implement MMMC as a representative of continuous-time finance methods. More complicated and advanced continuous-time finance methods are hard to implement for two reasons. First, to implement such methods, we need to estimate all the parameters of a multivariate SDE (like σ, v, μ and ω in Section 3.3). It is challenging since the derivation of likelihood requires solving multivariate stochastic integrals (Aït-Sahalia & Kimmel, 2010), Second, deriving explicit optimal policy functions is also difficult, which involves solving high-dimensional PDEs (like $k_2(t)$ and $k_3(t)$ in Lemma F.2). Further, such pure continuous-time models are expected to underperform, since they assume that the data exactly follows a parametric SDE and tend to underfit. This can also be seen by our comparison with CT-MB-RL (Section 5), which is a model-based RL method by relying on a Kim-Omberg model. As a result, we focus our empirical comparison to more competitive RL methods.

Note that FaLPO circumvents the two aforementioned challenges. First, our model calibration does not aim to fit all the parameters in an SDE, but only those related to learning θ_ϕ and θ_π. That is why our model calibration loss in Section 3.3 has such an easy-to-calculate form with the parameter θ_S as a simple vector. Second, FaLPO does not need a fully derived closed-form solution for the optimal policy. Like in Section 3.3, we use neural networks to parameterize $K(t)$ and $\phi()$, instead of fully deriving them like continuous-time finance methods. Being able to bridge this gap between continuous-time finance models and high multidimensional stock trading problems is one of our contributions.

L.6 Experiments with Transaction Costs

In this section, we consider the case with transaction costs. Usually, the cost of borrowing a stock to short can vary but typically ranges from 0.3% to 3% per year. Therefore, we take 1% annual transaction cost for short selling an asset. The fees are applied daily. Under this setting, we replicate our real-world experiments for the oil sector, using the same protocol. After the tuning procedure in Appendix L.3, the achieved results are reported in Table 13. The results are consistent with those without transaction costs.

Methods	Average Utility
FaLPO	$\mathbf{-2.25} \pm 1.649$
DDPG	-6.795 ± 0.8247
SLAC	-7.115 ± 0.8872
RichID	-6.365 ± 0.5989
CT-MB-RL	-5.57 ± 5.036

Table 13: Average terminal utility in oil sector with transaction costs

L.7 Experiment Results in Sharpe Ratio and Largest Drawdown

To provide a more thorough review for the real-world experiment, we provide the annual Sharpe ratio and maximum drawdowns [2] for the real-world experiments conducted in the mixed sector.

Methods	Sharpe Ratio	Largest Drawdown
FaLPO	**4.705**	-1105.046
DDPG	2.828	-4778.342
SLAC	0.6434	-5262.523
RichID	0.418	-643.062
CT-MB-RL	4.467	-993.661

Table 14: Annual Sharpe ratio and maximum drawdowns for the real-world experiments in the mixed sector

[2] A drawdown is the decline of a portfolio from a running historical maximum to a subsequent minimum.

FaLPO achieves superior Sharpe ratios compared to competing methods. However, we emphasize that utility is a more appropriate metric than returns or Sharpe ratios for portfolio optimization. Return alone is not a reliable metric for comparing portfolios, as it fails to account for risk. The utility function addresses this limitation by incorporating risk into the evaluation (see Figure 2). This is a critical feature in portfolio optimization. Utility is widely recognized as a foundational concept in portfolio optimization, underpinned by numerous seminal works (Merton, 1969). Many finance models explicitly rely on utility. To effectively leverage such models, utility becomes an indispensable metric. Portfolio optimization is defined as maximizing expected utility. Therefore, comparing methods based on other metrics (e.g., average returns or Sharpe ratio) may not be meaningful, as these metrics are not directly equivalent to utility. A policy excelling in utility may not necessarily yield high average returns or a high Sharpe ratio, as discussed in Appendix B. For this reason, our paper focuses on utility when comparing different methods.

L.8 Experiments with Different Initial Wealth

We vary the initial wealth in $\{3000, 5000, 8000, 1000\}$ for portfolio optimization using stocks in the oil sector following the same protocol as the experiments in Section 5.2. The results are summarized in Table 15. Specifically, FaLPO achieves superior performance to the competing methods with different initial wealth. Note that all the methods achieve higher terminal utility given more initial wealth.

Initial Wealth	3000	5000	8000	10000
FaLPO	$\mathbf{-21.08} \pm 16.775$	$\mathbf{-2.4} \pm 1.9$	$\mathbf{-0.243} \pm 0.1209$	$\mathbf{-0.03595} \pm 0.008896$
DDPG	-909.5 ± 3443.846	-6.6 ± 1.2	-0.34665 ± 0.01809	-0.046755 ± 0.00444
SLAC	-11865 ± 47260.664	-6.8 ± 0.2	0.35465 ± 0.07427	-0.04558 ± 0.00142
RichID	-45.51 ± 8.368	-6.5 ± 0.1	-0.33125 ± 0.009791	-0.045365 ± 0.0001446
CT-MB-RL	-28.715 ± 18.303	-4.2 ± 6.2	-0.30995 ± 0.1441	-0.043055 ± 0.002061

Table 15: Average terminal utility in oil sector with different initial wealth

L.9 Experiments with Different Continuous-Time Models

As demonstrated in Appendix F, FaLPO is compatible with various continuous-time financial models. In this section, we evaluate its performance on a real-world oil sector dataset, comparing results across three SDE families: the Merton model, the Kim–Omberg model, and the EVE model.

Sectors	**Average Utility**
Kim-Omberg	-2.4
Merton	-8.5
EVE	-2.5

L.10 Computation Time and Memory Usage

In this section, we report the memory usage and computation time of FaLPO. All experiments are conducted on AWS EC2 instances of type m5ad.24xlarge, using CPUs only. The experiments require less than 3 GB of CPU memory. The computation times are summarized in Figure 9.

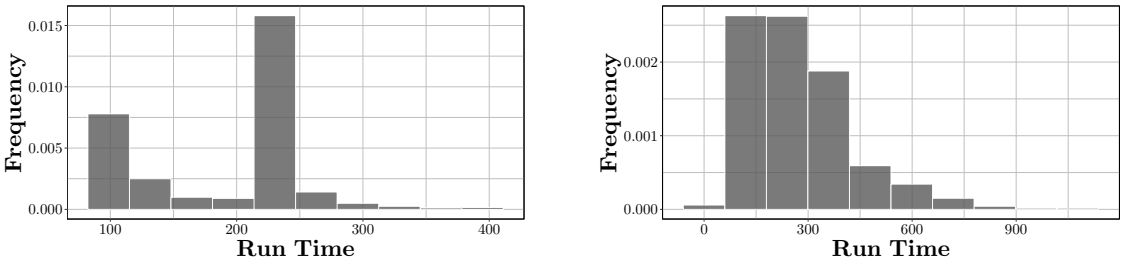

(a) Synthetic

(b) Real-World

Figure 9: Histograms for computation time of synthetic and real-world experiments under all the considered hyperparameters.

L.11 Performance of FaLPO over Different Market Regimes

As the market regime arguably changes before and after 2020, we delve deeper into the performance of FaLPO across these two periods. Specifically, we report the return and standard deviation of FaLPO on the oil sector before and after 2020 in Table 16. While a performance decline is observed after 2020, the decrease is relatively mild.

Period	Return (%)	Std (%)
Before 2020	7.8	2.8
After 2020	7.0	3.6

Table 16: Performance of FaLPO Before and After 2020